ACS OMEGA

Open Access

http://pubs.acs.org/journal/acsodf

Article

Valorizing Banana Peel Waste into Mesoporous Biogenic Nanosilica and Novel Nano-biofertilizer Formulation Thereof via Nano-biopriming Inspired Tripartite Interaction Studies

Ajay Kumar, Rishabh, Neetu Singh,* Yogendra K. Gautam, Priya, and Namrata Malik

Cite This: *ACS Omega* 2025, 10, 5537–5553

Read Online

ACCESS | Metrics & More | Article Recommendations | Supporting Information

ABSTRACT: The present study attempts to valorize banana peel waste (BPW) into high-value precipitated nanosilica-based agri-input. XRD analysis revealed smaller-sized biogenic nanosilica (BNS) with an increase (without heating) or decrease (with heating) in the duration of acid pretreatment during the pre-calcination step. The highest BNS yield was recorded in post-calcinated BPW ash involving simultaneous acid and heat treatment (1 h) (SA-3). FTIR analysis displayed an intense peak at 1078.3 cm^{-1}, indicating "Si–O–Si bond" asymmetric vibrations. FESEM-EDX micrographs revealed high-purity BNS of predominantly spheroid morphology. The BJH plot exhibited mesoporous nanosilica with a median pore diameter of ~33.82 nm. The bipartite interaction of 0.001 g mL^{-1} BNS signifies growth-promoting effects on *Bacillus subtilis* (BS) and *Raphanus sativus* (RS). The nano-primed RS seeds showed higher germination indices over non-primed seeds at 0.001 g of BNS mL^{-1}. Further, the nano-biopriming studies showed the synergistic response of BNS and BS interaction on RS seeds in terms of higher seedling growth, biomass content, and stress tolerance index. The findings open new avenues for developing nano-biofertilizer formulations that serve multifaceted functions such as waste management and biomass valorization into value-added products and fulfill sustainable development goals.

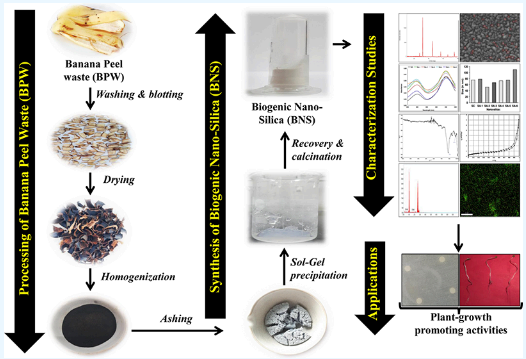

1. INTRODUCTION

Musa paradisiaca L. (*M. paradisiaca*), commonly known as banana, belongs to the family Musaceae, widely recognized as an edible fruit.[1] According to the FAO,[2] India is the largest banana producer (27.6 MT), followed by China (12.1 MT), the Philippines, and Brazil (6.9 MT).[3] Almost 60% of the banana fruit part, known as the peel, is discarded as waste.[4] Nearly 30–40% of banana production is vetoed as a consequence of poor quality standards, and the damage proportion to fruit during transportation is also very high.[1]

Fruit residues are one of the critical biowaste among different agricultural wastes.[3,5] Nearly 3.5 MT/year of banana peel waste (BPW) is produced globally by food industries.[3] According to another report, annually, ~114.08 MMT of banana waste loss is generated worldwide, despite significant hemicellulose, cellulose, and natural fibers contents. The conventional routes for disposing of fruit residues, like composting, burning, and landfilling,[6] can attract severe environmental consequences, including GHG emissions that could result in global climate change.[7]

As per reports, GHG emissions like carbon dioxide (CO_2), methane (CH_4), and nitrous oxide (N_2O) owing to waste disposal have increased by ~142, ~253, and ~121%, respectively.[3] Fruit wastes are the third source of GHG emissions in the USA and China.[2,3,8] According to Oelofse and Nahman,[9] each ton of fruit/food waste grossly generates ~4.14 tons of CO_2 via direct emissions or indirectly through microbial metabolism.[3] N_2O, CO_2, and CH_4 have also been defined as the main contributors to global warming, among which the former have more pronounced effects.[3,10–12]

Banana peel (BP) comprised ~30–40% of its fruit weight in total, with 60–65, 5–10, and 6–8% of cellulose, lignin, and hemicellulose, respectively.[3,11,13] In another study, BP's hemicellulose, lignin, and cellulose contents were ~11.87, ~7.3, and ~28.57%, respectively.[14] Apart from natural biopolymers, it contains proteins, lipids, dietary fibers, secondary metabolites (phenols, carotenoids, flavonoids, amine derivates, phytosterols, etc.),[1] and minerals (in mg/100 g) like sodium (~115.1), magnesium (~44.5), iron (~47), calcium (~59.1), phosphorus (~211.3), zinc (~0.033), copper (~0.51), manganese (~0.702), and potassium (~4.39).[15]

The rich biochemical profile of BPW[7] can be valorized into numerous value-added products such as biofuels, biofertilizers,

Received: September 4, 2024
Revised: October 27, 2024
Accepted: October 31, 2024
Published: February 5, 2025

and different nanomaterials.[6,16−19] Serna-Jiménez et al.[16] recorded 182 L_{CH_4}/(kg of volatile solids) via mesophilic biomethanation of BPW. Ruangtong et al.[20] demonstrated the reducing and capping potential of BPW crude extract in ZnO nanosheet synthesis. Naeem et al.[17] utilized BP fibers with bacterial cellulose to develop a reinforced composite with higher tensile strength and thermal stability. Other reported nanomaterials obtained from BPW are carbon quantum dots (~5 nm),[18] palladium NPs,[21] CuO/NiO nanocomposites,[22] silver NPs,[23] and titanium NPs.[24] The BPW-derived nanoparticles showed significant antibacterial, anticancer, drug-delivery, and dye degradation potential.[20,25−27] Therefore, nanotechnology-inspired valorization can be an attractive strategy for constructive mitigation of BPW into high-value products with multifarious utilities.

Many researchers have advocated nanosilica production from agro-industrial wastes.[6,28−34] Compared to chemical synthesis, biogenic nanosilica production has various advantages, such as being low-cost, energy-efficient, and eco-friendly.[35] Among different forms, the precipitated silica has growing industrial demand.[33] Nanosilica has applications in bio-imaging, biomedicine, biosensors, environmental remediation (recovery of heavy metals, nonmetals, radioactive compounds, oil, antibiotics, etc.), agriculture (stimulates the growth of beneficial soil microbes, facilitates toleranceto various abiotic stresses, develops resistance against different fungal and bacterial phytopathogens, regulates activities of antioxidant enzymes, promotes overall plant growth and development, etc.), catalysis, ceramics, optics, thin films, coatings, nanocomposites for construction materials, and use as anticorrosive, antimicrobial, and anticancer agent.[6,14,28,35−47]

The present study uses BPW as a precursor for green-chemistry routed biogenic nanosilica (BNS) extraction. The reaction conditions favoring BNS recovery were optimized. Further, the interaction studies of BNS with agriculturally beneficial bacteria (*Bacillus subtilis*) (BS) and *Raphanus sativus* (RS) seeds were performed to develop the novel nanosilica-based biofertilizer formulation with enhanced plant-growth-promoting activities.

2. EXPERIMENTAL SECTION

2.1. Chemicals and Raw Material. The chemicals employed in the present study, viz., 35−37% hydrochloric acid (maximum impurity levels, 0.0316%), sodium hydroxide (≥97% pure), sodium chloride (99.5% pure), 4% sodium hypochlorite (0.002% maximum impurity as manganese), and ethanol (99.9%), were of analytical grade and used without further purification. The preparation of reagents was performed in triple-distilled water (TDW), and glassware was thoroughly washed and sterilized for ~2 h at 180 °C.[48,49] BPW was procured from the nearby fruit juice corner, sorted, sliced into small pieces, and cleaned with tap water, followed by TDW. Further, the excess water from BPW slices was soaked using blotting sheets, completely dried at 60 °C, ground into fine powder form, and passed through a standard-size sieve to obtain a uniform particle size. The resultant powder was stored in an airtight jar until use.

2.2. Preliminary Analysis of BPW Powder. The BPW powder was subjected to ash, dry matter (DM), moisture, total organic carbon (TOC), and organic matter (OM) analyses.[50] Moisture (%) = $(P - Q/P) \times 100$; ash (%) = $R/P \times 100$; OM = $(Q - R/Q) \times 100$; TOC = OM/1.724, where 1.724 is the bemlen factor, and *P*, *Q*, and *R* are fresh weight biomass (FWB), weight obtained after 105 °C heat treatment for 6 h, and that followed by heating for another 6 h at 600 °C, respectively. An FTIR (PerkinElmer, L1600300) spectrum was recorded in the spectral range 4000 to 450 cm^{-1} to investigate the functional groups present in BPW powder.[49,51] Further, the aqueous extract of BPW powder was analyzed for the preliminary phytochemical analysis (i.e., alkaloids, phenols, flavonoids, carbohydrates, cardiac glycosides, tannins, quinones, terpenoids, phytosteroids, proteins, and amino acids),[52−57] and observations were marked as "+", "++", and "+++" for trace, moderate, and high concentrations, respectively.[52]

2.3. Extraction of BNS. Extraction of biogenic silica from agricultural residues typically involves sol−gel precipitation and alkaline−silica separation.[33] The major steps in the methodology adopted for the BNS synthesis from BPW are shown in Figure 1. First, the BPW powder (Section 2.1) was heated for 6 h at 650 °C in a muffle furnace to obtain ash. BPW ash undergoes acid leaching (1:10 (w/v)) for dissolving carbonate components[58] and removing metallic impurities.[59] Based on acid type, treatment duration, and heating process (80 °C), 7 BPW-ash treatments were designed, viz., SA-1, HCl washing for 1 h; SA-2, HCl washing for 3 h; SA-3, HCl washing for 1 h with heat treatment; SA-4, HCl washing for 3 h with heat treatment; SA-5, H_2SO_4 washing for 3 h; SA-6, HNO_3 washing for 3 h; SC, washing with distilled water for 3 h. The leached ash was left for 12 h in TDW under continuous stirring, followed by centrifuging at 4000 rpm for 30 min. The recovered ash containing silica undergoes alkali solubilization (3 N NaOH in 1:30 (w/v), 80 °C for 6 h in a hot water bath), resulting in sodium silicate formation, which is later precipitated at pH = 7, and heated at 80 °C for 2 h in a water bath. The obtained clear silica gel was aged for 24 h to recover the nanosilica.[60] The obtained nanosilica was washed with ethanol and TDW multiple times and calcinated at 100 °C for 6 h to obtain white BNS powder. The general reaction steps involved in HCl/NaOH-inspired extraction of nanosilica are depicted in the following reactions.[58]

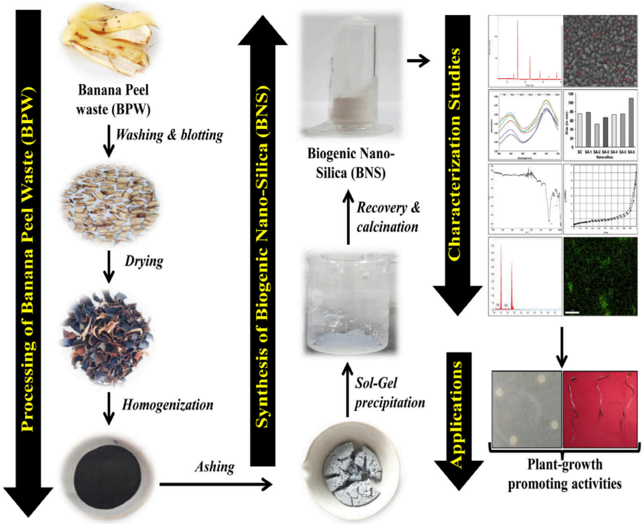

Figure 1. Schematic view indicating the synthesis and characterization of BNS.

https://doi.org/10.1021/acsomega.4c08152
ACS Omega 2025, 10, 5537−5553

$$SiO_2(\text{in BPW ash}) + 2HCl + H_2O \rightarrow H_2SiO_3 + 2H^+ + 2Cl^-$$

$$H_2SiO_3 + 2NaOH \rightarrow Na_2SiO_3 + 2H_2O$$

$$Na_2SiO_3 + 2HCl \rightarrow SiO_2(\text{extracted silica}) + 2NaCl + H_2O$$

2.4. Characterization of BNS. BNS was characterized for structural and optical properties. The phase and size of BNS were determined by X-ray diffractometer (Rigaku, Ultima IV) over the 2θ scanning range up to 80° (X-ray wavelength, i.e., Cu Kα anode = 0.15406 nm; tube current and voltage were 40 mA and 45 kV, respectively; scan speed = 8° min^{-1}).[61,62] The crystallite size (D) was determined using the Debye−Scherrer formula: "$k\lambda/\beta_{hkl}$ cos θ", where β_{hkl} = "full width at half-maximum" intensity value in radians; θ = peak position in radians, λ = 0.15406 nm, and k (constant) = 0.9.[61] The functional group associated with BNS was analyzed via an FTIR spectrophotometer (PerkinElmer, L1600300) in the transmission mode (4000 to 450 cm^{-1} spectral range).[63] The surface morphology and elemental composition of BNS were determined by "field emission scanning electron microscopy" (FE-SEM; TESCAN, MAGNA LMU), and "energy dispersive X-ray" (EDX) mapping (EDAX AMETEK, "Octane Elite Super EDS system"), respectively.[49,61,64] The particle size of nanosilica was determined with TEM (JEOL JEM 2100 PLUS). The absorption spectra of BNS aqueous dispersion were recorded at room temperature via UV−vis spectroscopy (ELICO 150) in the wavelength range from 250 to 400 nm.[61] Further, the recorded absorbance data were converted to estimate the band gap energy (E_g, in eV) from $E_g = hc/\lambda_{max}$, where $c = 3 \times 10^8$ m s^{-1} and $h = 4.135 \times 10^{-6}$ eV.[65] "Brunauer−Emmett−Teller" (BET) analysis (MicrotracBEL Corp., BELSORP-maxII (S/N: 175, Ver 2.0.1.1) was performed on BNS at adsorption temperature 77.355 K under nitrogen atmosphere to study the surface characteristics, i.e., pore diameter and volume through BET and "Barret−Joyner−Halenda" (BJH) plot using data analysis software (BELSORP, BELMaster, Ver 7.2.0.4).[66,67]

2.5. Maintenance of *B. subtilis* Culture. *Bacillus subtilis* (*B. subtilis*; Gram positive (Gram +ve) bacteria) were maintained in nutrient broth (NB) of the following composition (w/v): peptone (0.5%), yeast extract (0.2%), NaCl (0.5%), and beef extract (0.1%). pH was attuned at ~7.4. For solid media plates, 2% (w/v) agar was added to the above NB composition. The nutrient medium was autoclaved for 15 min under 15 lbs of pressure and 121°C temperature, followed by cooling at room temperature (RT) before use. For experimental studies, *B. subtilis* cell suspension maintained at active log phase (inoculated into NB media followed by incubating at 37 °C for overnight) was considered.[61,68−70]

2.6. Disk Diffusion Assay (DDA) and Growth Kinetics Study. The freshly prepared nutrient media were poured into Petri plates and solidified for nearly 30 min. *B. subtilis* cell culture (BCC) was spread over solidified media plates. The sterile disks of filter paper nearly 6 mm in diameter were dipped in the variable treatment doses of BNS prepared in aqueous solution (until saturation) and equidistantly placed on the inoculated plates. The disks dipped in TDW served as a negative control. The inoculated media plates were incubated in a BOD incubator at 37 °C for a 24 h duration. Serial dilutions for colony count of *B. subtilis* (cultured in NB with and without BNS) were performed on nutrient agar media, and plates were incubated as mentioned for DDA.[71,72] For bacterial growth kinetics studies, the BCC maintained at the logarithmic phase was first diluted to obtain optical density (OD) of about 0.1 at 600 nm (equivalent to ~10^8 CFU mL^{-1}) and then grown at 37 °C in NB media (with and without BNS). The turbidity measurements were performed using a UV−vis spectrophotometer (OD at 600 nm).[61,73−76]

2.7. Seed Germination Assay. *Raphanus sativus* (L.) (*R. sativus*; radish) was chosen as a model plant in the present study due to its rapid growth and higher germination rate.[61] The uniform-sized healthy seeds of radish were surface sterilized using sodium hypochlorite solution (2.5% (w/v))[61] for ~5 min and then washed thrice with sterile TDW. Five seeds were placed equidistantly on the Petri dish equipped with a sterile filter paper soaked with 4 mL of the test sample or TDW (served as a control). The prepared Petri dishes were then incubated at 25 ± 1 °C in the dark[77] for ~7 days, and germination data were recorded upon the emergence of the radicle (~2 mm)[78] beyond the seed coat. The growth indices were measured for germination percentage (G, %), seedling length (SL),[79] fresh weight (FWB), and dry weight biomass (DWB),[80] vigor index (VI-I and -II),[81,82] and stress tolerance index (STI) for seedling parameters such as radicle length (RL), plumule length (PL), SL, FWB, and DWB.[83,84]

$$G\ (\%) = \frac{\text{no. of germinated seeds}}{\text{no. of tested seeds}} \times 100$$

$$\text{VI-I} = G \times \text{SL}$$

$$\text{VI-II} = \text{DWB} \times \text{SL}$$

$$\text{STI}\ (\%) = \frac{\text{seedling parameter of stress treatment}}{\text{seedling parameter of control}} \times 100$$

The experiments were carried out in triplicates in a "complete randomized design"; the recorded mean values of independent triplicate trials were denoted as mean ± SD.[61] We have performed a "Pearson correlation coefficient (r) analysis" to study the association between investigated germination indices under variable treatments, and the r-value closer to +1 or −1 indicated a "strong positive correlation" or "strong negative correlation", respectively.[61,85]

2.8. Antioxidant Assay. Total phenol content (TPC) was determined as per Khatiwora et al.[86] with slight modifications. Germinated seedlings of radish (GSH) were extracted in 80% (v/v) ethanol, and the volume was marked up to 3 mL with TDW. In the next step, 0.5 mL of FC reagent (1:1 with TDW) was added, followed by 2 mL of 20% sodium carbonate. The test sample was heated for ~2 min and cooled at RT, and the absorbance was recorded using a UV−vis spectrophotometer at 650 nm wavelength. The curve was plotted against the gallic acid standard, and TPC was expressed as "mg of GAE equivalent/(g of sample)". Total flavonoid content (TFC) was determined, as mentioned in Baba and Malik,[87] with few modifications. A 1 mL aliquot of ethanolic extract of GSH was added to 4 mL of TDW, followed by 0.3 mL of aqueous solution of 5% sodium nitrite and incubated at RT for 5 min. Next, 0.3 mL of aqueous aluminum chloride solution (10%) was added to the test sample and incubated for 6 min at RT, and then 2 mL of 1 M aqueous NaOH solution was added and the volume marked up to 10 mL with TDW. The absorbance was recorded using a UV−vis spectrophotometer at 510 nm

https://doi.org/10.1021/acsomega.4c08152
ACS Omega 2025, 10, 5537−5553

Table 1. Preliminary Phytochemical Analysis of the Powdered BPW Aqueous Extract

Compound	Test	Result[a]	Observation
Alkaloids	Mayer	++	Whitish/cream colored precipitate
	Wagner	+++	Reddish-brown precipitate
Phenols	$FeCl_3$	+	Intense color
Flavonoids	Lead acetate	++	Yellow precipitate
	Alkaline reagent	+	Intense-yellow color
Carbohydrates	Fehling's	+	Yellowish/brownish-red precipitate
	Molish	−	Violet color not appearing at the junction of two-liquid layers
Proteins and amino acids	Biuret	++	Purplish-violet/pinkish-violet color
	Xanthoprotic	++	Yellow precipitate
	Ninhydrin	−	Blue/Purple color not appeared
Cardiac glycosides	Keller-Kiliani	+	Reddish brown color at junction of two-liquid layers and upper layer appeared bluish green
Tannins	Lead acetate	+++	Yellow precipitate
Quinones	Acid precipitation	++	Red precipitate
Terpenoids	Salkowski	+	Red-brown precipitate
Phytosteroids	Hesse's reaction	+	Chloroform layer red and acid layer greenish-yellow

[a]Concentrations: "+" = trace, "++" = moderate, and "+++" = high.

wavelength. The curve was plotted against the quercetin standard, and TFC was expressed as "mg of quercetin equivalent per g of sample".

A hydrogen peroxide (H_2O_2) assay on GSH was performed as per Yahyaoui et al.[88] with slight modifications. Briefly, the GSH was homogenized in 5 mL of 0.1% (w/v) chilled trichloroacetic acid (TCA), incubated for ∼30 min at RT, and centrifuged to collect the supernatant. To 1.0 mL of the test sample, equal volumes (2 mL each) of potassium phosphate buffer (10 mM, pH 7) and 1 M potassium iodide were added. The absorbance was recorded at wavelength 390 nm, and H_2O_2 content was determined from the extinction coefficient value of 0.28 mM^{-1} cm^{-1}. A lipid peroxidation assay to determine the malondialdehyde (MDA) content was performed according to Iftikhar and Perveen[89] with slight modifications. A 1 mL aliquot of supernatant (prepared as mentioned in the H_2O_2 assay) was added to 4 mL of 0.5% thiobarbituric acid (prepared in 20% TCA) and heated at ∼95 °C for ∼30 min, followed by cooling at RT. The absorbance was recorded at wavelengths 600 and 532 nm. MDA content (nmol/mL) was calculated using $[(\text{absorbance}_{532} - \text{absorbance}_{600})/155000] \times 10^6$.[90]

3. RESULTS AND DISCUSSION

3.1. Characterization of BPW Powder. BPW showed moisture, DM, OM, and TOC contents (weight %) of 90.82 ± 1.90, 9.18 ± 1.90, 83.60 ± 0.62, and 48.19 ± 0.86, respectively. As per the reports, these parameters can be varied depending on the plant variety, prevailing environmental conditions, etc.[91,92] The ash content in BPW was 15.85 ± 0.67%, which is in agreement with the previous findings.[93,94] The EDX (Oxford Instruments) analysis of BPW showed "Si" and "O" contents (weight %) of 6.67 and 26.54, respectively. The reported elemental impurities were Mg, P, S, Cl, K, Ca, Mn, Rb, Nb, and Pb[95] (Supporting Information Figure S1). Preliminary phytochemical analysis of the aqueous BPW extract showed the presence of alkaloids, phenols, flavonoids, carbohydrates, cardiac glycosides, tannins, quinones, terpenoids, phytosteroids, proteins, and amino acids (Table 1). Previous studies mentioned most of these metabolites in banana peel's aqueous/organic solvent extracts.[96−99]

FTIR spectra of BPW powder show peaks at 2919.47, 2851.2, 1602.8, 1379.2, 1245, 1038.02, and 895.27 cm^{-1} (Figure 2a). The peaks recorded for BPW ash were at 2988.27, 1985, 1448.3, 1045.7, 880.4, and 702.16 cm^{-1} (Figure 2b). Similar records were documented in earlier studies. Memon et al.[100] in FTIR analysis of banana peel powder, observed peaks at 884.6, 1035.2, 1613.6, 1734, 2850.6, and 2920.3 cm^{-1} corresponding to NH amine deformation, CO stretching of ester/ether, OH bending, carboxylate stretching, CO, and CH stretching of ester/COOH, respectively. In another work, Udochukwu and Akpoviri[101] noted peaks at 2919.47 and 895.27 cm^{-1} in BPW powder, showing CH-stretching vibrations of $CH_3/CH_2/CH$ groups, and carbohydrates and water deformation, respectively. The peaks in ash samples at 702.16 cm^{-1} correspond to C═C bending and C−Cl stretching, 1045.7 cm^{-1} indicated S═O and C−F stretching, and 1448.3 cm^{-1} designated calcium oxide, while calcite phases are suggested by 2988.27, and 880.4 cm^{-1}.[102−104]

3.2. Synthesis and Recovery of BNS. The key reaction steps involved in the synthesis and recovery of BNS are shown in Figure 3.[19] The effect of pretreatment conditions with respect to (wrt) acid type, treatment duration, and temperature on BNS recovery was investigated. The silica yield (in %) was calculated as per the following equation.[105]

$$\text{silica yield (\%)} = \frac{\text{weight of silica recovered}}{\text{weight of BPW ash}} \times 100$$

The BNS yields were recorded from experimental trials carried out in triplicate. The BNS content was highest at SA-3, followed by SA-2, indicating favorable effects of heat treatment and substantial reductions in reaction time. Compared to SA-6, the BNS recovery was greater in the case of SA-5 but lower than SA-2, which preferred pretreatment of ash with HCl for 3 h over HNO_3 and H_2SO_4 (Figure 4). Overall, compared to the control (SC), 59.5, 46.1, 39.9, 38.3, 38, and 22.8% higher BNS yields were noted in treatment samples SA-3, SA-2, SA-6, SA-4, SA-1, and SA-5, respectively. Adebisi et al.[106] also reported higher Si contents in maize stalks treated with HCl before (pre-calcination) and after ashing (post-calcination).

3.3. Characterization of BNS. *3.3.1. XRD.* XRD diffractogram showed significant peaks at 2θ angles 27.2−27.3, 31.5−31.7, 45.3−45.4, 53.7−53.8, 56.3−56.4, 66.0−66.2, and 75.1−75.2° (Figure 5a−g). BNS samples SA-2 to SA-5 also demonstrated additional peaks at 28.1−28.5, 40.3−40.7, 50−

https://doi.org/10.1021/acsomega.4c08152
ACS Omega 2025, 10, 5537−5553

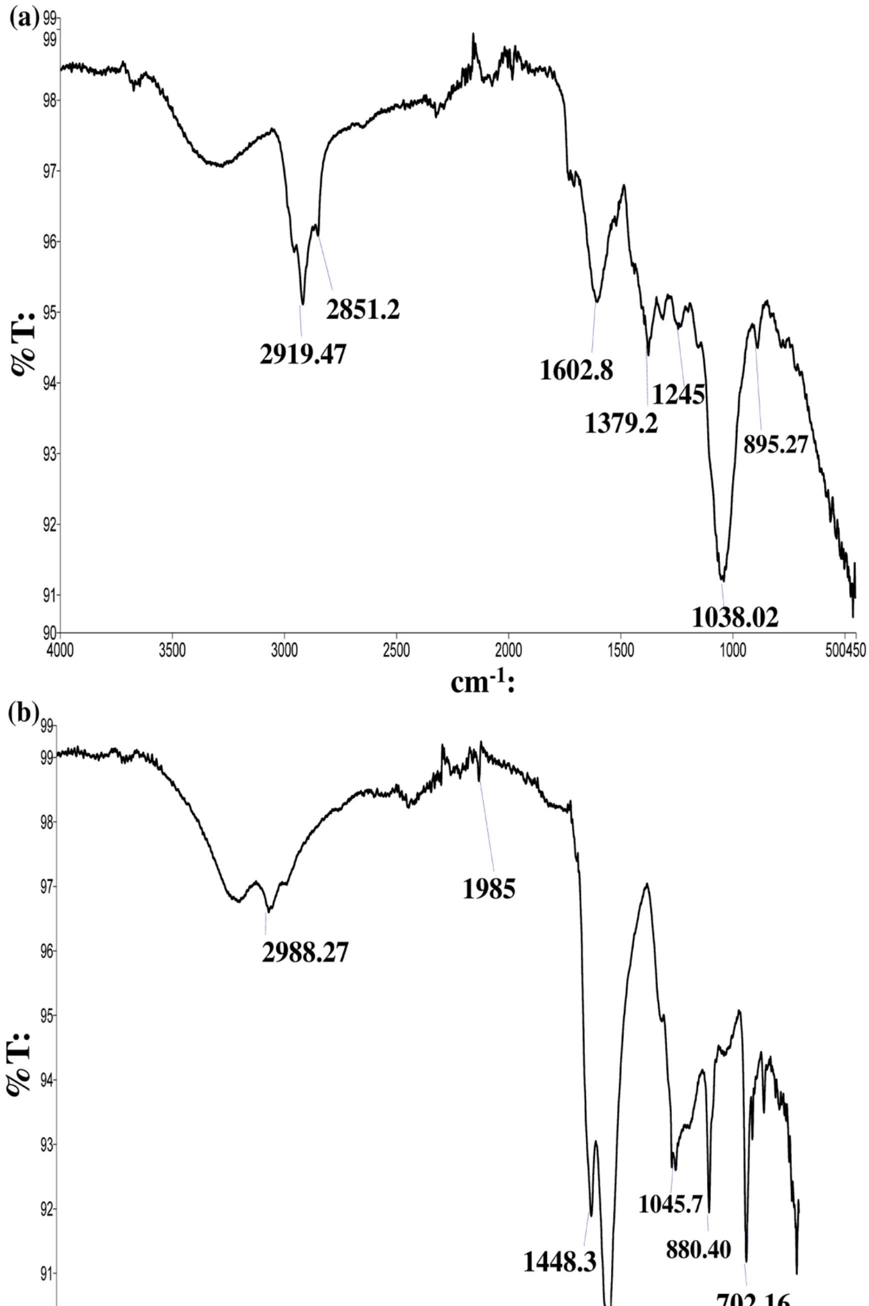

Figure 2. FTIR spectra of BPW: (a) homogenized dried powder and (b) ash.

50.5, 58.5−59, 66.0−66.9, 72.8−72.9, and 83.4−83.8°. Similar peaks were reported in earlier studies by Barma et al.[107] (2θ = 27, 31, 45, 56, 75, and 84°), Ali et al.[108] (2θ = 40.3, and 53.9°), Silmi et al.[109] (2θ = 50.14°), and Periakaruppan et al.[110] (2θ = 28°) for SiO_2. The HCl pretreated ash (HPA) for 3 h duration (with and without heat treatment) favored smaller-sized BNS than those obtained from HNO_3 and H_2SO_4 treated samples. Further, the short heating duration (SHD) of HPA (SA-3) resulted in reduced-sized BNS compared to the long heating duration (LHD) (SA-4). SA-1 and SA-6 exhibited a higher BNS size than the control (SC) (Figure 5h). Overall, the crystallite size (CS) of BNS obtained at different reaction conditions ranges from ∼51 to 78 nm (except SA-6), which is in concordance with the previous report (Table S1).[58] The pretreatment duration and temperature have significant effects on the size of BNS. XRD results demonstrated a decrease in BNS size with an increase (without heating) or a decrease (with heating) in the HCl preatment duration for ash. Dislocation density (δ) was calculated from the CS (D) of BNS using equation $\delta = 1/D^2$ to study the defects in SiO_2 crystal structure.[111] "δ" indicates the degree of crystallization and decreases with an increase in BNS size.[61,111] The microstrain (ε_a) was determined as per equation "$\varepsilon_a = \beta$ cos

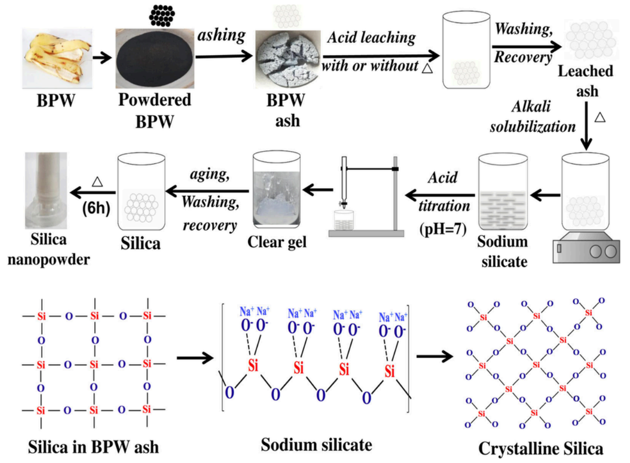

Figure 3. Key reaction steps involved in synthesis and recovery of BNS (conceptualized from ref 19).

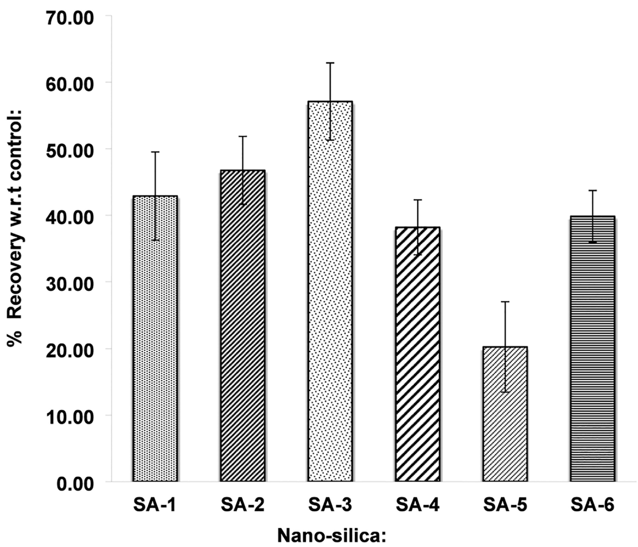

Figure 4. Recovery of BNS under different reaction conditions. (Error bar indicates mean ± SD.)

$\theta/(4 \times 10^{-3})$" and displayed an increasing trend in proportion with the "δ" values.[112]

3.3.2. UV–Vis Spectroscopy and FTIR. FTIR spectra peaks of BNS (SA-3) at 1078.3 and ∼850 cm^{-1}, corresponding to the "Si–O–Si bond" asymmetric vibrations.[63,113] The peak at 586.23 cm^{-1} also indicates Si–O elements.[110] The minor peaks at 1500–2000 and ∼3400 cm^{-1} are indicative of absorbed water molecules bending and silanol or H–O–H stretching, respectively (Figure 6b).[67,114] The optical properties of nanosilica are based on variable defects due to the partial formation of the "Si–O–Si tetrahedral network" ("O" and "Si" vacancies).[115] UV–vis spectra of BNS synthesized at different reaction conditions showed maximum absorbance (λ_{max}) at ∼260 nm (Figure 6a).[114] The prominent peaks were also noticed at ∼300 nm.[116] The band gap corresponding to λ_{max} at 260 nm was ∼4.77 eV.[117,118]

3.3.3. FE-SEM, TEM, and EDX. FE-SEM micrographs indicated predominantly spheroid morphology of BNS (SA-3), which was further confirmed in TEM investigation (Figure 7a,e).[119,120] The particle size calculated from TEM analysis was ∼68–170 nm. EDX mapping revealed elemental composition (weight %) of ∼31 and ∼69 "Si" and "O", respectively (Figure 7b,c). The atomic percentages of "Si" and "O" were ∼20, and ∼80%, respectively. However, the elemental composition may vary with the choice of template and extraction process adopted.[58] Joni et al.[121] synthesized SiO_2 nanoparticles with elemental "Si" and "O" contents of ∼38 and ∼62%, respectively. Stanley and Nesaraj[122] reported 56.63 and 43.37 wt % "O" and "Si", respectively, in nanosilica (synthesized without surfactant).

3.3.3.4. BET Analysis. The nitrogen adsorption–desorption curve of BNS (SA-3) displayed type-IV isotherm according to IUPAC classifications (Figure 7d).[64] The total pore volume (p/p_o = 0.990) obtained from the BET plot was 0.01 cm^3 g^{-1}. Alhadhrami et al.[58] reported a pore volume of 0.062 cm^3 g^{-1} for biogenic silica extracted from RH. In another study, Araichimani et al.[123] obtained a pore volume of 0.094 cm^3 g^{-1} from BJH analysis for RH-derived nanosilica. The pore volume can be varied with the substrate material (precursor), operational conditions during the extraction process, and crystallinity of nanosilica.[108,124–127] Idris et al.[124] found lower pore volume for crystalline nanosilica (0.0021^a and 0.0045^b cm^3 g^{-1}) compared to amorphous nanosilica (0.678^a and 0.327^b cm^3 g^{-1}) derived from corncobs[a] and olive stones[b]. Ramasamy et al.[125] from wheat straw ash derived amorphous nanosilica with a micropore volume of 0.013 cm^3 g^{-1}. The BJH plot of BNS (SA-3) revealed mesoporous nanosilica with average and median pore diameters of ∼19.55 and ∼33.82 nm, respectively,[60,128,129] and surface area of ∼2.16 m^2g^{-1}.

3.4. Effect of BNS on Bacterial Growth. To explore BNS and BS as a novel combination for plant-growth-promoting (PGP) activities, we first investigated the effect of direct BNS (SA-3) treatment on BS. For this purpose, disc diffusion assay (DDA) and bacterial growth kinetics (BGK) studies were performed (Figure 8). No ZOI was noticed at 0.001 g (T1) and 0.01 g of BNS mL^{-1} (T2), indicating no apparent inhibitory effect of treatment doses on BS growth. Previously, Ferrusquia-Jiménez et al.[40] did not find any toxicity effects of 0.0001 g of nanosilica mL^{-1} against "*Bacillus cereus*-Amazcala" (B.c-A.). For cell viability analysis, colony count was performed, and the CFUs recorded for T1 and T2 showed ∼16.8 and ∼12.5% increments compared to the control. The findings of BGK studies allow for determining the bacterial cell density (BCD) and the toxicity of NPs in a liquid medium.[61] The absorbance values recorded at 600 nm (OD_{600}) showed higher BCD in T1 than in the control. However, T2 displayed lower OD_{600} values compared to those of the control. Overall, the findings signify that the BNS treatment up to 0.001 g mL^{-1} could have growth-promoting effects on BS. Karunakaran et al.[45] reported an increase in the growth of four PGP rhizobacteria (PGPRs) (*Pseudomonas fluorescens*, *Bacillus brevis*, *Azotobacter vinelandii*, and *Bacillus megaterium*) by >20% upon nanosilica treatment. They noted doubling in PGPRs CFUs ($\times 10^8$) counts (g^{-1} of soil) from 4 to 8.

The mechanism of SiO_2 adsorption on the cell surface of Gram-positive bacteria is typically governed by the presence of teichoic (TEA) and teichuronic acid (TUA) in the cell wall[130] (Figure 9). TEA and TUA contain phosphate and carboxylate groups, respectively, that aid negative charge to the bacterial cell surface (BCS) and facilitate SiO_2 binding.[130] In some bacteria, proteins (SiP) also played a significant role in SiO_2 uptake.[45] Studies also mentioned that the hydration property of silica could facilitate its attraction on the bacterial surface.[45] Tian et al.[131] reported the possibility of SiO_2 interaction with

https://doi.org/10.1021/acsomega.4c08152
ACS Omega 2025, 10, 5537–5553

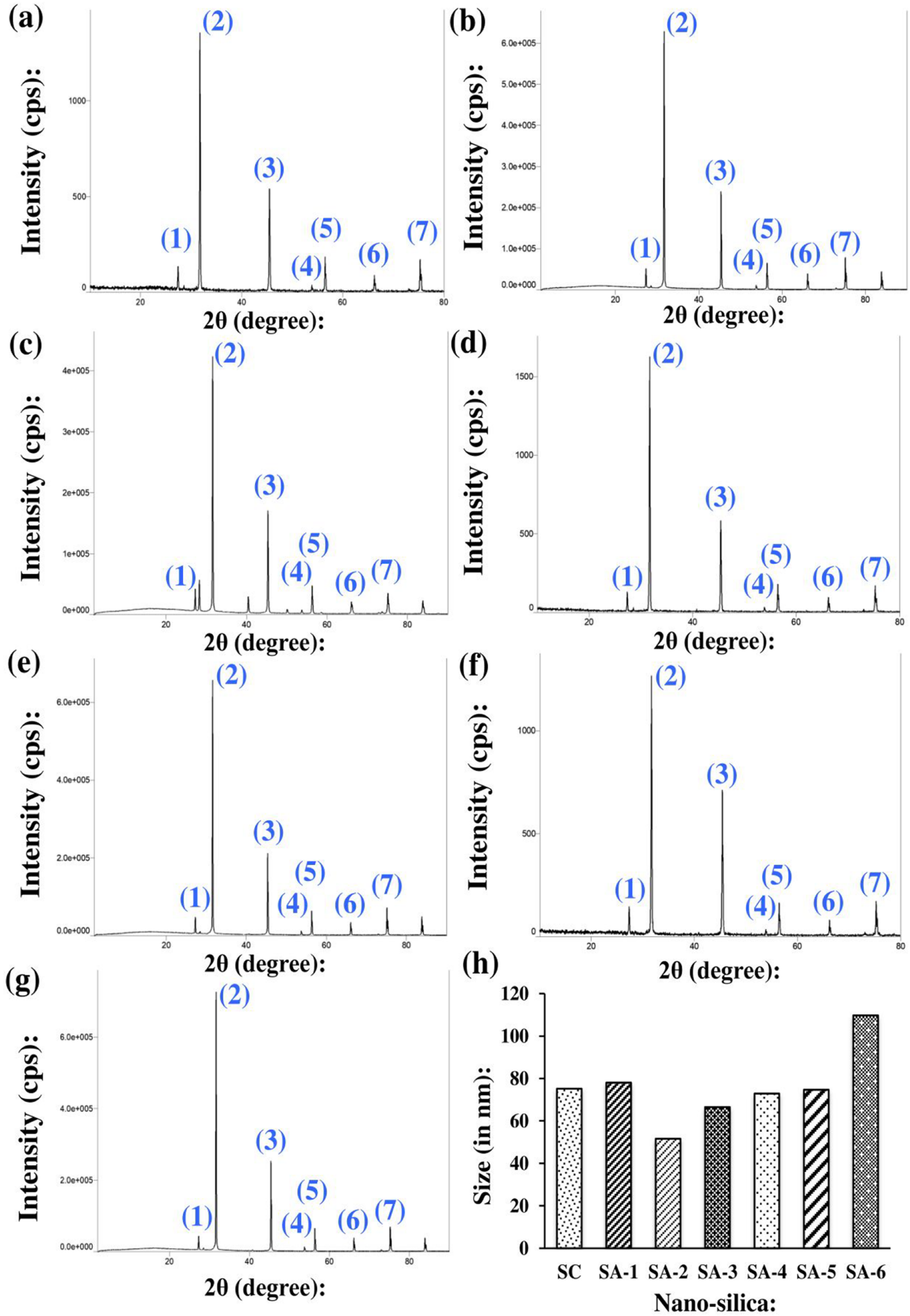

Figure 5. XRD spectra of BNS: (a) SC, (b) SA-1, (c) SA-2, (d) SA-3, (e) SA-4, (f) SA-5, (g) and SA-6. (h) Size of BNS obtained from Scherrer–Debye equation (nos. 1–7 showing peak positions corresponding to 2θ angles: ~27.2–27.3, ~31.5–31.7, ~45.3–45.4, ~53.7–53.8, ~56.3–56.4, ~66.1–66.2, and 75.1–75.3°, respectively).

BCS-associated proteins in a few bacteria via hydrogen bonding with amino acid residues.

3.5. Effect of BNS on Seed Germination. Figure 10 shows the general mechanism of silica uptake by the plants. In soil application, silicic acid is the major available form of silica and is taken by roots via passive or active transport. Transport proteins (LSi) play an essential role in the active transport of silica. Silica is deposited in vascular bundles as phytoliths, and in plants such as grasses, it forms a secondary cuticle-Si protective layer. SiNPs, in the case of foliar application, gain

https://doi.org/10.1021/acsomega.4c08152
ACS Omega 2025, 10, 5537–5553

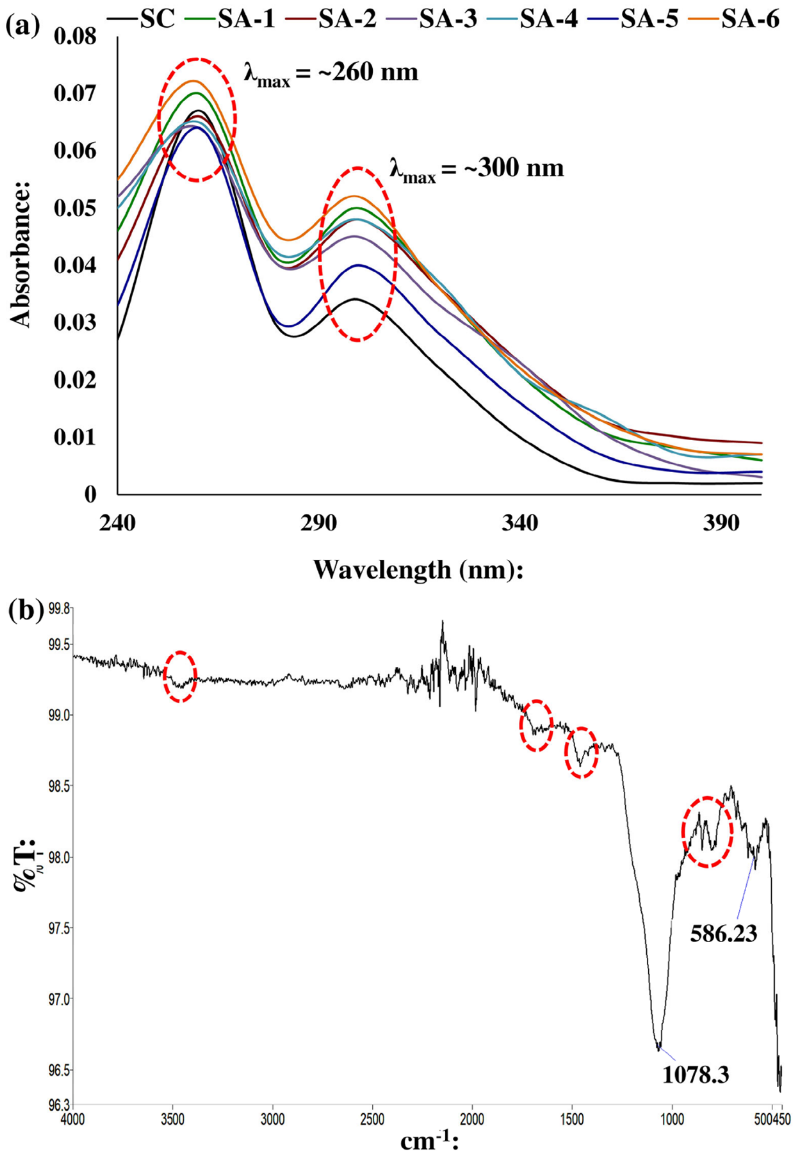

Figure 6. (a) UV−vis spectra showing characteristic absorption peaks of BNS synthesized at different reaction conditions. (b) FTIR spectra showing characteristic functional groups in BNS (SA-3).

entry into leaves via cuticle (through penetration or diffusion) or stomatal pores and translocated to roots via phloem.

In the present study, RS seeds exposed to filter papers soaked with 0.001 (Te) and 0.01 (Tf) g BNS mL^{-1} (nonpriming experiments) showed lower germination indices compared to the control. However, RL and RLTI values were higher in "Te" than "Tf" and control. In the case of seeds nanoprimed with 0.001 g mL^{-1} BNS (Tc), higher PL, RL, SL, FWB, VI, and stress tolerance indices were obtained than those of control, "Te", "Tf", and "Td". Also, the marginal increment in *G* (%) and DWB was recorded in control over "Te". Studies reported growth-prompting effects of nanosilica on several crops like wheat, tomato, sugar cane, maize, rice, soybean, potato, etc., which help to alleviate abiotic stress such as salinity, heavy metal, heat, drought, etc.[37,38,136,137]

The comparative assessment of nanopriming and non-priming experiments indicated growth-promoting effects of seed nanoprimed with 0.001 g of BNS mL^{-1} (Tc), which concords with previous reports.[138] Sun et al.[138] recorded an improvement in phyto-biomass, seed germination, chlorophyll, and protein contents in wheat and lupin at mesoporous nanosilica concentrations of 0.0005 and 0.001 g mL^{-1}. Zaheer et al.[139] also found an increase in plant height and biomass weight in *Vigna radiata* (L.) after application of nanosilica (0.002, 0.0002, and 0.000002 mg L^{-1}) on 6 days old plants, compared to control. Karunakaran et al.[45] noted 100% seed germination in maize in the case of nanosilica treatment, as against 97, and 95% in microsilica and control experiments, respectively. Elamawi et al.[42] performed a foliar application of 0.00005 mg L^{-1} nanosilica on *Fusarium fujikuroi* infested rice seedlings and witnessed an increase in grain yield and a reduction in bakanae disease symptoms. We observed that "Tf" exhibited lower germination indices than the control, "Te", "Td", and "Te", indicating phytotoxicity of direct BNS exposure at elevated doses on RS seeds.

3.6. Tripartite Interaction Studies. The tripartite interaction of RS seeds with BS (biopriming) followed by BNS (nano-biopriming) showed a synergistic response in terms of seedling growth, biomass content, vigor indices, and stress tolerance potential. The nano-biopriming using 0.001 g

https://doi.org/10.1021/acsomega.4c08152
ACS Omega 2025, 10, 5537−5553

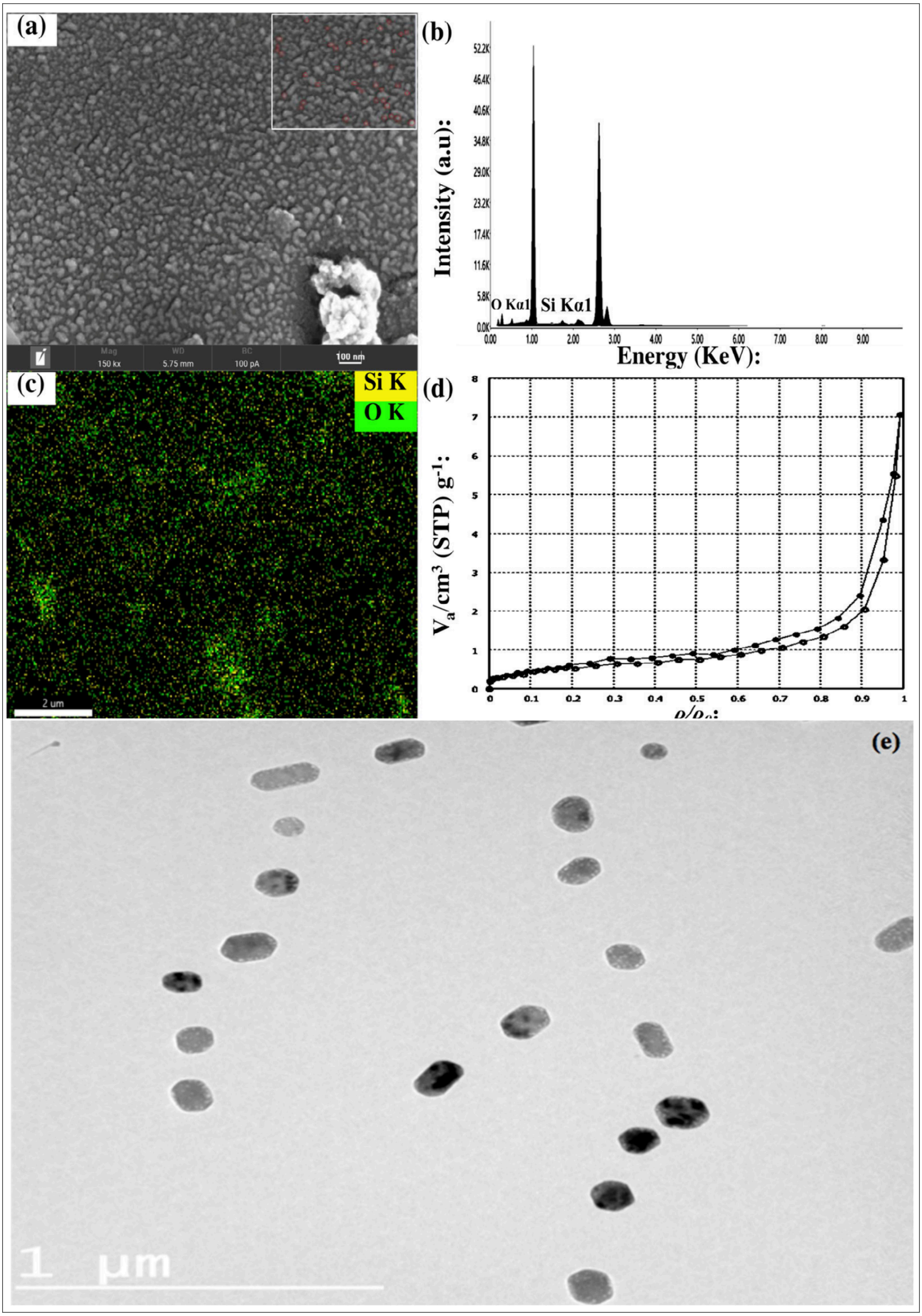

Figure 7. (a) FESEM micrograph at 150k× magnification (100 nm scale) (Inset: enlarged view showing spheroid morphology.) (b) EDX spectra (c) Elemental color mapping from EDX (d) Nitrogen adsorption−desorption isotherm curve (e) TEM image (at 1 μm scale) of BNS (SA-3).

https://doi.org/10.1021/acsomega.4c08152
ACS Omega 2025, 10, 5537−5553

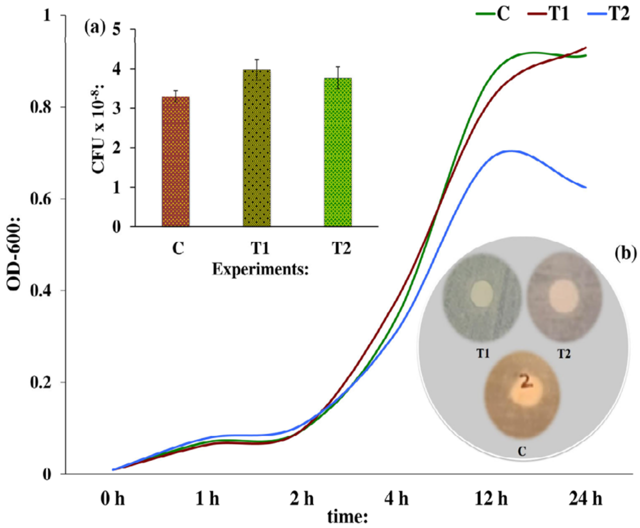

Figure 8. Growth kinetics curve of *B. subtilis* (insets: (a) CFU count; (b) disc diffusion assay results at different treatment doses of BNS) (C = control, T1 = 0.001 g of BNS mL^{-1}, and T2 = 0.01 g of BNS mL^{-1}).

of BNS mL^{-1} (Ta) indicated ∼21, ∼27.5, ∼23.9, ∼17, ∼12.4, ∼16.5, and ∼35% higher PL, RL, SL, FWB, DWB, VI-2, and VI-2, respectively, compared to control (Figure 11a,b). PL, SL, FWB, DWB, and VI-2 also showed increments in "Ta" seedlings with respect to "Td" (nanopriming using 0.001 g of BNS mL^{-1}). These values, coupled with higher tolerance indices in "Ta", favored the growth-promoting effects of combined BS−BNS treatment over solitary treatment of BNS (Figure 11e). Ferrusquia-Jiménez et al.[40] performed co-application of B.c-A. and 0.0001 g mL^{-1} of nanosilica on chili pepper plants and observed increments in leaves number,

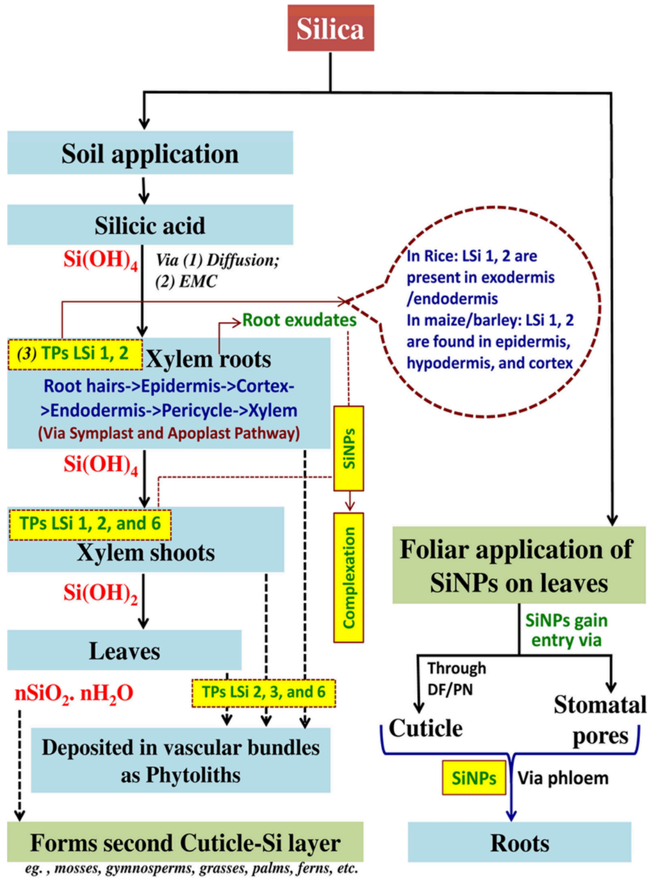

Figure 10. Mechanism of silica uptake by plants (conceptualized from refs 35, 37, and 140−143) (SiNPs, silica nanoparticles; EMC, excess mass infiltration; DF, diffusion; PN, penetration; TPs, transport proteins).

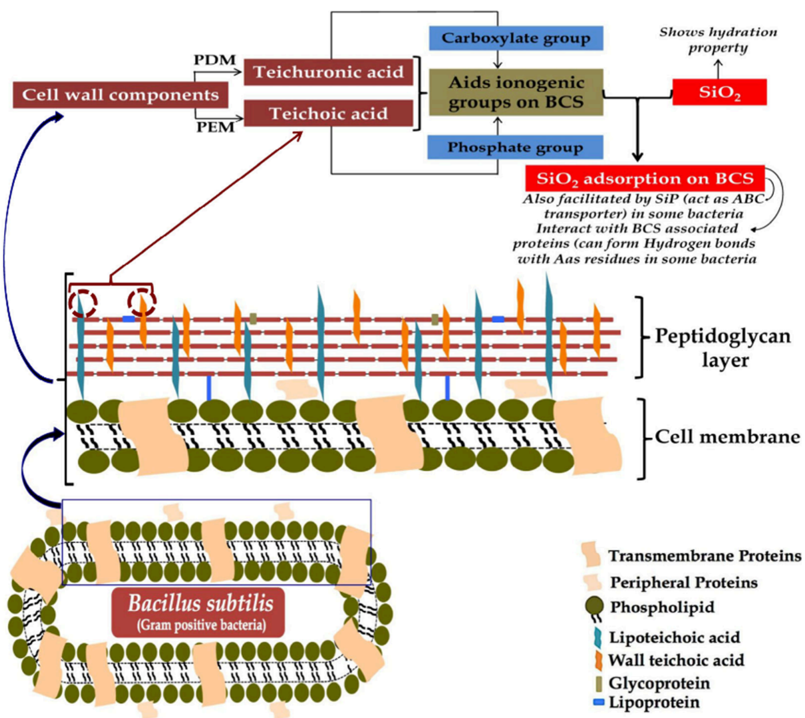

Figure 9. Probable mechanism of silica adsorption by *B. subtilis* (conceptualized from refs 45 and 130−135) (BCS, bacterial cell surface; PEM, phosphate enriched media; PDM, phosphate deficit media; SiP, silica induced protein; ABC, ATP-binding cassette; Aa, amino acid).

https://doi.org/10.1021/acsomega.4c08152
ACS Omega 2025, 10, 5537−5553

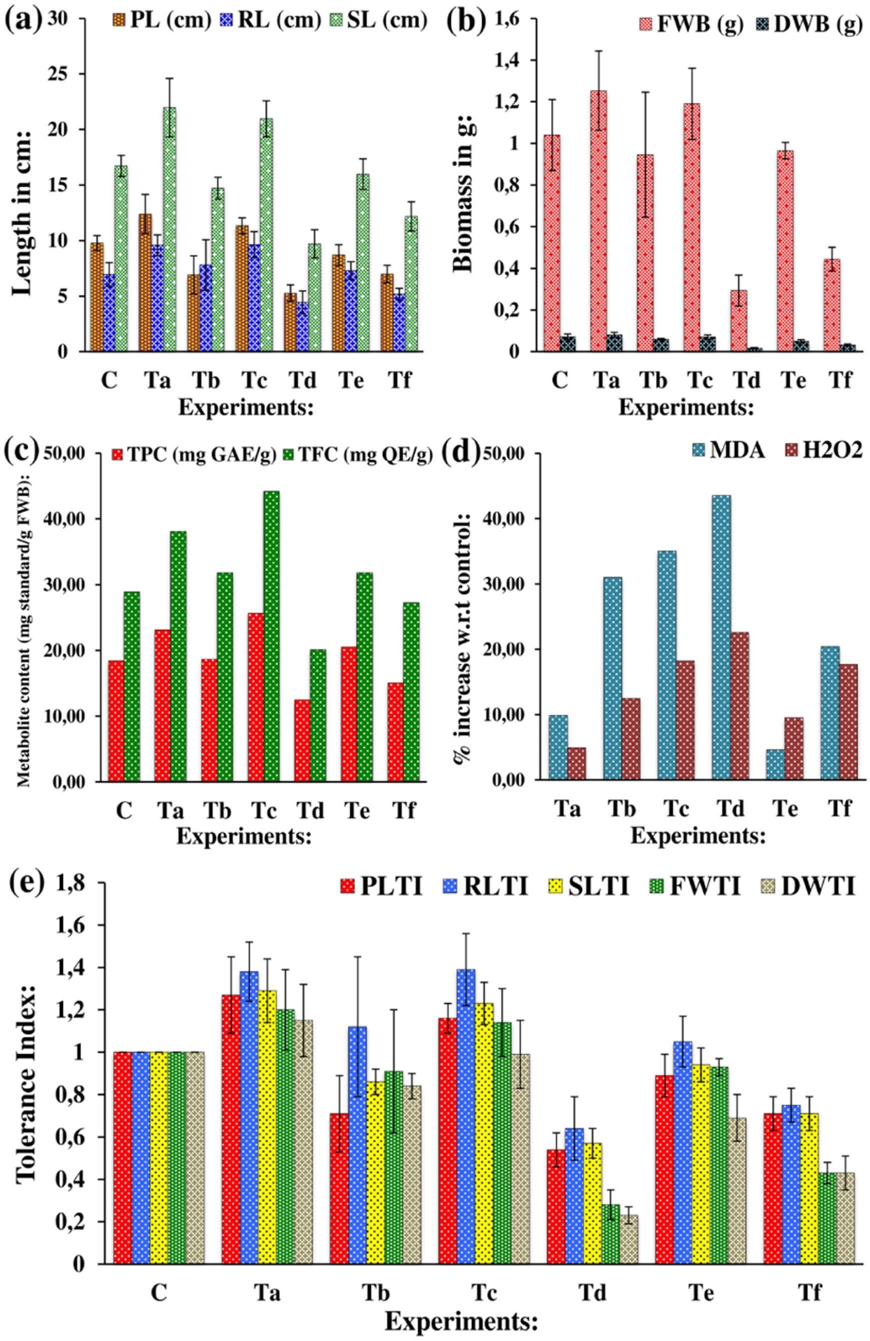

Figure 11. Effect of BNS and BS treatments on (a) seedling length and (b) biomass content. Antioxidant activity: (c) total phenol and flavonoid contents and (d) hydrogen peroxide and malonaldehyde content. (e) Stress tolerance indexes for different growth parameters (Ta = BS/0.001 g of BNS mL^{-1} (priming), Tb = BS/0.01 g of BNS mL^{-1} (priming), Tc = 0.001 g of BNS mL^{-1} (priming), Td = 0.01 g of BNS mL^{-1} (priming), Te = 0.001 g of BNS mL^{-1} (nonpriming), and Tf = 0.01 g of BNS mL^{-1} (nonpriming); error bars indicate mean ± SD).

G (%) of seeds, plant height, yield, and number of fruits.[40] Except for RL, we found that all of the germination indices values were lower in treatment "Tb" (nano-biopriming using 0.01 g of BNS mL^{-1}) compared to control (Figure 11a,b). The data recorded for "Tb" and "Tf" when compared to control, "Ta", and "Td" demonstrated phytotoxicity at a higher dose of BNS (0.001 g mL^{-1}) irrespective of treatment mode. An integration of biopriming along with BNS treatment displayed positive interaction with RS seeds and supported PGP activities together with stress tolerance potential. In this way, the effective dose of BNS has also been reduced substantially, hence promoting judicious use of agri-inputs, keeping sustainable agricultural practices in view. Table 2 shows strong positive correlation between SL-PL, SL-PL, FWB-RL, and FWB-DWB ($R^2 \geq 0.95$); DWB-RL, DWB-SL, and SL-FWB ($0.94 \geq R^2 \geq 0.90$); and PL-RL, PL-FWB, and PL-DWB ($R^2 \leq 0.89$).

3.7. Antioxidant Activities. TPC and TFC were estimated for "treated" and "control" RS seedlings. "Ta", and "Tc" showed ∼20.3 and ∼28.2% higher TPC and ∼24.1 and ∼34.6% higher TFC, w.r.t. control, respectively (Figure 11c). The results promoted nanopriming and nano-biopriming of seeds using BNS (0.001 g of BNS mL^{-1}) over other treatments and control. Sun et al.[138] observed no oxidative stress up to

https://doi.org/10.1021/acsomega.4c08152
ACS Omega 2025, 10, 5537−5553

Table 2. Correlation Analyses between the Recorded Germination Indices of *R. sativus*[a]

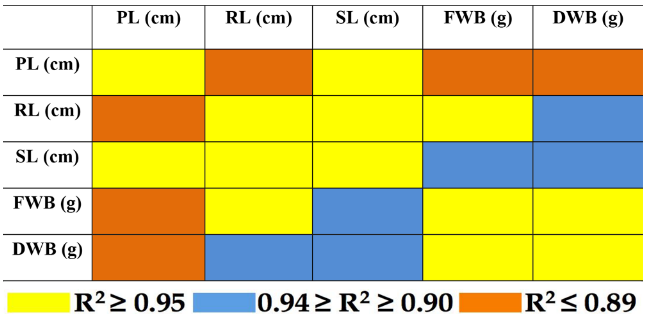

[a]Note: Growth parameters were recorded for experimental trials "C", and "Ta" to "Tf".

0.002 g mL^{-1} of nanosilica and recommended for applications in plants over the tested range. Even Ferrusquía-Jiménez et al.[40] noted defense-associated response of nanosilica (0.0001 mg L^{-1})/B.c-A. co-application in chili pepper plant in terms of higher superoxide dismutase and catalase activities. The H_2O_2 content analysis demonstrated higher values in the following treatments (compared to control): Td (~22.6%) > Tc (~18.2%) > Tf (~17.7%) > Tb (~12.5%) (Figure 11d). MDA contents showed ~43.6, ~35.1, ~31, and ~20.4% increments in "Td", "Tc", "Tb", and "Tf", respectively, w.r.t. control, indicating significant stress at elevated doses of BNS, precisely at direct seed treatment (Td) (nanopriming).

3.8. Credit of BNS for Long-Term Agricultural Applications. To ascertain the suitability of developed BNS for long-term agricultural applications, we have performed interaction studies of BNS with BS and RS. The bipartite interaction of BNS with *B. subtilis* (BS) showed no obvious toxicity at both of the tested doses (i.e., 0.001 and 0.01 g mL^{-1}). The increase in CFU counts at 0.001 g of BNS mL^{-1} was in agreement with the previous reports. Karunakaran et al.[45] observed the growth-promoting effects of nanosilica against four PGP rhizobacteria. Their seed germination studies also revealed no phytotoxicity symptoms and oxidative stress in RS at 0.001 g of BNS mL^{-1}. Despite this, we have witnessed the synergistic response of BNS and BS interaction on germination indices, tolerance index, and antioxidant levels of RS.[40] However, to better understand the credit of nanosilica for long-term applications, we recommend additional investigations exploring their effect of introduction on the environment during agriculture applications via foliar spraying or soil fertigation.

3.9. Economic Analysis. As per the "Nano Silica Market Research" report, the nanosilica market from USD ($) 4.6 billion (valued in 2021) is expected to reach $8.6 billion by the year 2031, rising at a 6.5% CAGR from 2022 to 2031.[144] We have encountered few reports on the cost−benefit analysis of biogenic nanosilica production. Maroušek et al.[115] extracted nanosilica from coir-pith via an acid-based sol−gel method and projected cost valued at 1.3 Euros (€)/g (expenses breakup owing to energy, reactants, feedstock and processing, labor, equipment depreciation, and others were 0.2, 0.3, 0.1, 0.2, 0.4, and 0.1 €, respectively) against the wholesale market price of about 2.4−3.3 €/g. Singh et al.[67] estimated *Sapindus mukorossi* seed extract stabilized nanosilica production cost of $24.19 per kg (expenses breakup include the cost of paddy straw, *S. mukorossi* seeds, chemicals, labor, energy, and capital) from paddy straw ash against the market price of ~$198 per kg, with net profit of about $173.81 per kg. These figures suggest the tremendous feasibility of commercial nanosilica production by exploring various low-cost precursor substrates.

4. CONCLUSIONS

Banana peel waste has been successfully utilized as a low-cost precursor substrate for developing biogenic nanosilica (BNS). The highest BNS yield at SA-3 directed toward favorable effects of heat treatment and a significant reduction in reaction time. The obtained BNS was of comparable grade as those per previous reports on silica extraction from rice straw, sugar cane bagasse, etc. XRD crystallite and TEM particle sizes were ~66.52 and ~68−170 nm, respectively, and FTIR analysis revealed silanol functional groups. The average pore diameter calculated from the BJH plot was ~19.55 nm. Overall, BNS (SA-3) characterization studies confirmed the nanosized, mesoporous structure with a predominantly spheroid morphology. The findings instate positive tripartite interaction of seeds with *B. subtilis*/BNS (SA-3) that can be productively translated into the growth-promoting novel nano-biofertilizer formulation. The study potentially served as a stepping stone toward green chemistry routed facile, cost-effective, eco-benign, and energy-efficient biogenic silica production exploiting various phytobiomass-derived agro-industrial waste. It is anticipated that the recorded observations could facilitate the concerned stakeholders engaged in the area of biomass valorization and rural development toward the productive materialization of plenteous agricultural residues into a comprehensive platform catering to waste management, generating high-value products, and promoting a circular bioeconomy in the purview of sustainable development goals.

■ ASSOCIATED CONTENT

Data Availability Statement

The data underlying this study are available in the published article and its Supporting Information.

Supporting Information

The Supporting Information is available free of charge at https://pubs.acs.org/doi/10.1021/acsomega.4c08152.

(Figure S1) EDX analysis of BPW; (Table S1) XRD crystallite size of biogenic nanosilica obtained at different reaction conditions (PDF)

■ AUTHOR INFORMATION

Corresponding Author

Neetu Singh − *Department of Biotechnology, Mewar Institute of Management, Ghaziabad, Uttar Pradesh 201012, India;* orcid.org/0000-0001-6352-4643; Email: neetu.avni@gmail.com

Authors

Ajay Kumar − *Department of Biotechnology, Mewar Institute of Management, Ghaziabad, Uttar Pradesh 201012, India; Department of Biotechnology, Mewar University, Chittorgarh, Rajasthan 312901, India*

Rishabh − *Department of Biotechnology, Mewar Institute of Management, Ghaziabad, Uttar Pradesh 201012, India*

Yogendra K. Gautam − *Smart Materials and Sensor Laboratory, Department of Physics, Ch. Charan Singh University, Meerut, Uttar Pradesh 250004, India;* orcid.org/0000-0003-4662-4583

https://doi.org/10.1021/acsomega.4c08152
ACS Omega 2025, 10, 5537−5553

Priya − *Department of Biotechnology, Mewar Institute of Management, Ghaziabad, Uttar Pradesh 201012, India*
Namrata Malik − *Department of Biotechnology, Mewar Institute of Management, Ghaziabad, Uttar Pradesh 201012, India*

Complete contact information is available at:
https://pubs.acs.org/10.1021/acsomega.4c08152

Author Contributions

A.K.: Conceptualization, investigation, writing—original draft, review and editing, and supervision. R.: Experimental, writing—original draft, and literature survey. N.S.: Overall supervision and writing−review and editing. Y.K.G.: Writing—review and data interpretation; P.: Experiment. N.M.: Supervision.

Funding

No funding was received to assist with the preparation of this manuscript.

Notes

The authors declare no competing financial interest.

■ ACKNOWLEDGMENTS

The authors are grateful to the CRF, IIT Delhi, for FE-SEM, EDX mapping, and BET; CIF, Jamia Millia Islamia (New Delhi), for XRD; Professor Shailendra S. Gaurav, Department of Genetics & Plant Breeding, CCSU (Meerut) for FTIR; and Sprint testing solutions, Nagpur for TEM and EDX facilities. The support given by all during the study is acknowledged, and the authors are thankful to all who dedicated themselves by all means. Errors, if any, are purely unintentional. We attempted to acknowledge the copyright holders of all matters reproduced in this work.

■ REFERENCES

(1) Hikal, W. M.; Said-Al Ahl, H. A. H.; Bratovcic, A.; Tkachenko, K. G.; Sharifi-Rad, J.; Kačániová, M.; Elhourri, M.; Atanassova, M. Banana Peels: A Waste Treasure for Human Being. *Evidence-Based Complementary and Alternative Medicine* **2022**, *2022*, 1−9.

(2) *Food Wastage Footprint: Impacts on Natural Resources: Summary Report*; Natural Resources Management and Environment Department, Food and Agriculture Organization of the United Nations (FAO): Rome, Italy, 2013. https://www.fao.org/3/i3347e/i3347e.pdf (accessed 2024-03-22).

(3) Sial, T. A.; Khan, M. N.; Lan, Z.; Kumbhar, F.; Ying, Z.; Zhang, J.; Sun, D.; Li, X. Contrasting Effects of Banana Peels Waste and Its Biochar on Greenhouse Gas Emissions and Soil Biochemical Properties. *Process Safety and Environmental Protection* **2019**, *122*, 366−377.

(4) Alzate Acevedo, S.; Diaz Carrillo, A. J.; Flórez-López, E.; Grande-Tovar, C. D. Recovery of Banana Waste-Loss from Production and Processing: A Contribution to a Circular Economy. *Molecules* **2021**, *26*, 5282.

(5) Peerzada, J. G.; Chidambaram, R. A Statistical Approach for Biogenic Synthesis of Nano-Silica from Different Agro-Wastes. *Silicon* **2021**, *13* (7), 2089−2101.

(6) Yadav, M.; Dwibedi, V.; Sharma, S.; George, N. Biogenic Silica Nanoparticles from Agro-Waste: Properties, Mechanism of Extraction and Applications in Environmental Sustainability. *Journal of Environmental Chemical Engineering* **2022**, *10* (6), No. 108550.

(7) Farooq, M.; Anwar, R.; Shukat, R.; Qamar Abbas, S.; Ilyas, N.; Cristina, M.; Wang, Y. Y. Ecofriendly utilization of by products from banana peel in food production and other industrial applications. A review. *Carpathian J. Food Sci. Technol.* **2021**, *13* (4), 149−157.

(8) Eckard, R.; DPI Victoria; The University of Melbourne. *Greenhouse Gas Emissions From Agriculture—Reduction Options*, 2010. http://www.greenhouse.unimelb.edu.au/pdf_files/Hamilton_Field_Day2010.pdf (accessed 2024-03-22).

(9) Oelofse, S. H.; Nahman, A. Estimating the Magnitude of Food Waste Generated in South Africa. *Waste Manag Res.* **2013**, *31* (1), 80−86.

(10) Hu, M.; Chen, D.; Dahlgren, R. A. Modeling Nitrous Oxide Emission from Rivers: A Global Assessment. *Global Change Biology* **2016**, *22* (11), 3566−3582.

(11) Pokharel, P.; Kwak, J.-H.; Ok, Y. S.; Chang, S. X. Pine Sawdust Biochar Reduces GHG Emission by Decreasing Microbial and Enzyme Activities in Forest and Grassland Soils in a Laboratory Experiment. *Science of The Total Environment* **2018**, *625*, 1247−1256.

(12) Montzka, S. A.; Dlugokencky, E. J.; Butler, J. H. Non-CO2 Greenhouse Gases and Climate Change. *Nature* **2011**, *476* (7358), 43−50.

(13) Liew, R. K.; Nam, W. L.; Chong, M. Y.; Phang, X. Y.; Su, M. H.; Yek, P. N. Y.; Ma, N. L.; Cheng, C. K.; Chong, C. T.; Lam, S. S. Oil Palm Waste: An Abundant and Promising Feedstock for Microwave Pyrolysis Conversion into Good Quality Biochar with Potential Multi-Applications. *Process Safety and Environmental Protection* **2018**, *115*, 57−69.

(14) Manivannan, H.; Krishnamurthy, A.; Macherlla, R.; Chidambaram, S.; Pandiaraj, S.; Muthuramamoorthy, M.; Ethiraj, S.; Kumar, G. M. Enhancing the Silica-Magnetic Catalyst-Assisted Bioethanol Production from Biowaste via Ultrasonics. *Clean Technol. Environ. Policy* **2023**, DOI: 10.1007/s10098-023-02638-5

(15) Hassan, H. F.; Hassan, U. F.; Usher, O. A.; Ibrahim, A. B.; Tabe, N. N. Exploring the Potentials of Banana (Musa Sapietum) Peels in Feed Formulation. *Int. J. Adv. Res. Chem. Sci.* **2018**, *5*, 10−14.

(16) Serna-Jiménez, J. A.; Luna-Lama, F.; Caballero, Á.; Martín, M. D. L. Á.; Chica, A. F.; Siles, J. Á. Valorisation of Banana Peel Waste as a Precursor Material for Different Renewable Energy Systems. *Biomass and Bioenergy* **2021**, *155*, No. 106279.

(17) Naeem, M. A.; Siddiqui, Q.; Khan, M. R.; Mushtaq, M.; Wasim, M.; Farooq, A.; Naveed, T.; Wei, Q. Bacterial Cellulose-Natural Fiber Composites Produced by Fibers Extracted from Banana Peel Waste. *Journal of Industrial Textiles* **2022**, *51*, 990S−1006S.

(18) Atchudan, R.; Jebakumar Immanuel Edison, T. N.; Shanmugam, M.; Perumal, S.; Somanathan, T.; Lee, Y. R. Sustainable Synthesis of Carbon Quantum Dots from Banana Peel Waste Using Hydrothermal Process for in Vivo Bioimaging. *Physica E: Low-dimensional Systems and Nanostructures* **2021**, *126*, No. 114417.

(19) Ghani, U.; Hussain, S.; Ali, A.; Tirth, V.; Algahtani, A.; Zaman, A.; Mushtaq, M.; Althubeiti, K.; Aljohani, M. Hydrothermal Extraction of Amorphous Silica from Locally Available Slate. *ACS Omega* **2022**, *7* (7), 6113−6120.

(20) Ruangtong, J.; T-Thienprasert, J.; T-Thienprasert, N. P. Green Synthesized ZnO Nanosheets from Banana Peel Extract Possess Anti-Bacterial Activity and Anti-Cancer Activity. *Materials Today Communications* **2020**, *24*, No. 101224.

(21) Bankar, A.; Joshi, B.; Kumar, A. R.; Zinjarde, S. Banana Peel Extract Mediated Novel Route for the Synthesis of Palladium Nanoparticles. *Mater. Lett.* **2010**, *64* (18), 1951−1953.

(22) Kaur, J.; Rani, S. CuO/NiO Nano-Composite Synthesized from Banana Peels for Grow Light. *Materials Today: Proceedings* **2023**, *91*, 1−6.

(23) Bankar, A.; Joshi, B.; Kumar, A. R.; Zinjarde, S. Banana Peel Extract Mediated Novel Route for the Synthesis of Silver Nanoparticles. *Colloids Surf., A* **2010**, *368* (1−3), 58−63.

(24) Hameed, R. S.; Fayyad, R. J.; Nuaman, R. S.; Hamdan, N. T.; Maliki, S. A. J. Synthesis and Characterization of a Novel Titanium Nanoparticles Using Banana Peel Extract and Investigate Its Antibacterial and Insecticidal Activity. *J. Pure Appl. Microbiol* **2019**, *13* (4), 2241−2249.

(25) Sengupta, A.; Sarkar, A. Synthesis and Characterization of Nanoparticles from Neem Leaves and Banana Peels: A Green Prospect for Dye Degradation in Wastewater. *Ecotoxicology* **2022**, *31* (4), 537−548.

(26) Ibrahim, H. M. M. Green Synthesis and Characterization of Silver Nanoparticles Using Banana Peel Extract and Their Antimicrobial Activity against Representative Microorganisms. *Journal of Radiation Research and Applied Sciences* **2015**, *8* (3), 265−275.
(27) Gopi, D.; Kanimozhi, K.; Bhuvaneshwari, N.; Indira, J.; Kavitha, L. Novel Banana Peel Pectin Mediated Green Route for the Synthesis of Hydroxyapatite Nanoparticles and Their Spectral Characterization. *Spectrochimica Acta Part A: Molecular and Biomolecular Spectroscopy* **2014**, *118*, 589−597.
(28) Noor, U.; Soni, S.; Purwar, S.; Gupta, E. Sustainable Valorization of Food Waste for the Biogeneration of Nanomaterials. In *Green and Sustainable Approaches Using Wastes for the Production of Multifunctional Nanomaterials*; Elsevier, 2024; pp 91−101.
(29) Chaudhary, S.; Jain, V. P.; Sharma, D.; Jaiswar, G. Implementation of Agriculture Waste for the Synthesis of Metal Oxide Nanoparticles: Its Management, Future Opportunities and Challenges. *J. Mater. Cycles Waste Manag* **2023**, *25* (6), 3144−3160.
(30) Pal, D. B.; Tiwari, A. K. *Agricultural and Kitchen Waste: Energy and Environmental Aspects*, 1st ed.; CRC Press: Boca Raton, FL, 2022. DOI: 10.1201/9781003245773.
(31) Ahmed, M. M.; Badawy, M. T.; Ahmed, F. K.; Kalia, A.; Abd-Elsalam, K. A. Fruit Peel Waste-to-Wealth: Bionanomaterials Production and Their Applications in Agroecosystems. In *Agri-Waste and Microbes for Production of Sustainable Nanomaterials*; Elsevier, 2022; pp 231−257. DOI: 10.1016/B978-0-12-823575-1.00001-9.
(32) Elemike, E. E.; Ekennia, A. C.; Onwudiwe, D. C.; Ezeani, R. O. Agro-Waste Materials: Sustainable Substrates in Nanotechnology. In *Agri-Waste and Microbes for Production of Sustainable Nanomaterials*; Elsevier, 2022; pp 187−214. DOI: 10.1016/B978-0-12-823575-1.00022-6.
(33) Utama, P. S.; Yamsaengsung, R.; Sangwichien, C. Production and Characterization of precipitated silica from palm oil mill fly ash using CO_2 impregnation and mechanical fragmentation. *Braz. J. Chem. Eng.* **2019**, *36* (1), 523−530.
(34) Sangeetha, J.; Thangadurai, D.; Hospet, R.; Purushotham, P.; Manowade, K. R.; Mujeeb, M. A.; Mundaragi, A. C.; Jogaiah, S.; David, M.; Thimmappa, S. C.; Prasad, R.; Harish, E. R. Production of Bionanomaterials from Agricultural Wastes. In *Nanotechnology*; Prasad, R., Kumar, M., Kumar, V., Eds.; Springer: Singapore, 2017; pp 33−58. DOI: 10.1007/978-981-10-4573-8_3.
(35) Sharma, P.; Prakash, J.; Kaushal, R. An Insight into the Green Synthesis of SiO2 Nanostructures as a Novel Adsorbent for Removal of Toxic Water Pollutants. *Environmental Research* **2022**, *212*, No. 113328.
(36) Kamboj, R.; Bains, A.; Sharma, M.; Kumar, A.; Ali, N.; Parvez, M. K.; Chawla, P.; Sridhar, K. Green Synthesis of Rice Straw-Derived Silica Nanoparticles by Hydrothermal Process for Antimicrobial Properties and Effective Degradation of Dyes. *Process Safety and Environmental Protection* **2024**, *185*, 1049−1060.
(37) Goswami, P.; Mathur, J.; Srivastava, N. Silica Nanoparticles as Novel Sustainable Approach for Plant Growth and Crop Protection. *Heliyon* **2022**, *8* (7), No. e09908.
(38) Larkunthod, P.; Boonlakhorn, J.; Pansarakham, P.; Pongdontri, P.; Thongbai, P.; Theerakulpisut, P. Synthesis and Characterization of Silica Nanoparticles from Rice Husk and Their Effects on Physiology of Rice under Salt Stress. *Chil. j. agric. res.* **2022**, *82* (3), 412−425.
(39) Periakaruppan, R.; S, M. P.; C, P.; P, R.; S, G. R.; Danaraj, J. Biosynthesis of Silica Nanoparticles Using the Leaf Extract of Punica Granatum and Assessment of Its Antibacterial Activities Against Human Pathogens. *Appl. Biochem. Biotechnol.* **2022**, *194* (11), 5594−5605.
(40) Ferrusquía-Jiménez, N. I.; González-Arias, B.; Rosales, A.; Esquivel, K.; Escamilla-Silva, E. M.; Ortega-Torres, A. E.; Guevara-González, R. G. Elicitation of Bacillus Cereus-Amazcala (B.c-A) with SiO2 Nanoparticles Improves Its Role as a Plant Growth-Promoting Bacteria (PGPB) in Chili Pepper Plants. *Plants* **2022**, *11* (24), 3445.
(41) Jeelani, P. G.; Mulay, P.; Venkat, R.; Ramalingam, C. Multifaceted Application of Silica Nanoparticles. A Review. *Silicon* **2020**, *12* (6), 1337−1354.
(42) Elamawi, R. M.; Tahoon, A. M.; Elsharnoby, D. E.; El-Shafey, R. A. Bio-Production of Silica Nanoparticles from Rice Husk and Their Impact on Rice Bakanae Disease and Grain Yield. *Archives of Phytopathology and Plant Protection* **2020**, *53* (9−10), 459−478.
(43) Roohizadeh, G.; Majd, A.; Arbabian, S. The effect of sodium silicate and silica nanoparticles on seed germination and growth in the Vicia faba L. *Trop. Plant Res.* **2015**, *2*, 85−89.
(44) Suriyaprabha, R.; Karunakaran, G.; Kavitha, K.; Yuvakkumar, R.; Rajendran, V.; Kannan, N. Application of Silica Nanoparticles in Maize to Enhance Fungal Resistance. *IET nanobiotechnol.* **2014**, *8* (3), 133−137.
(45) Karunakaran, G.; Suriyaprabha, R.; Manivasakan, P.; Yuvakkumar, R.; Rajendran, V.; Prabu, P.; Kannan, N. Effect of Nanosilica and Silicon Sources on Plant Growth Promoting Rhizobacteria, Soil Nutrients and Maize Seed Germination. *IET nanobiotechnol.* **2013**, *7* (3), 70−77.
(46) Makarovsky, I.; Boguslavsky, Y.; Alesker, M.; Lellouche, J.; Banin, E.; Lellouche, J.-P. Novel Triclosan-Bound Hybrid-Silica Nanoparticles and Their Enhanced Antimicrobial Properties. *Adv. Funct. Mater.* **2011**, *21* (22), 4295−4304.
(47) Wang, L.; Zhao, W.; Tan, W. Bioconjugated Silica Nanoparticles: Development and Applications. *Nano Res.* **2008**, *1* (2), 99−115.
(48) Vikal, S.; Gautam, Y. K.; Meena, S.; Parewa, V.; Kumar, A.; Kumar, A.; Meena, S.; Kumar, S.; Singh, B. P. Surface Functionalized Silver-Doped ZnO Nanocatalyst: A Sustainable Cooperative Catalytic, Photocatalytic and Antibacterial Platform for Waste Treatment. *Nanoscale Adv.* **2023**, *5* (3), 805−819.
(49) Verma, L. M.; Kumar, A.; Bashir, A. U.; Gangwar, U.; Ingole, P. P.; Sharma, S. Phase Controlled Green Synthesis of Wurtzite (*P* 63 *Mc*) ZnO Nanoparticles: Interplay of Green Ligands with Precursor Anions, Anisotropy and Photocatalysis. *Nanoscale Adv.* **2023**, *6* (1), 155−169.
(50) Sharma, K.; Kumar, A.; Sharma, R.; Singh, N. Exploring integrated methodology for phytoremediation and biofuel production potential of Eichhornia crassipes. *Indian J. Biochem. Biophys.* **2022**, *59*, 368−375.
(51) Sagar, N. A.; Khar, A.; Vikas; Tarafdar, A.; Pareek, S. Physicochemical and Thermal Characteristics of Onion Skin from Fifteen Indian Cultivars for Possible Food Applications. *Journal of Food Quality* **2021**, *2021*, 1−11.
(52) Shaikh, J. R.; Patil, M. Qualitative Tests for Preliminary Phytochemical Screening: An Overview. *Int. J. Chem. Stud.* **2020**, *8* (2), 603−608.
(53) Dahanayake, J. M.; Perera, P. K.; Galappatty, P.; Melshandi Perera, H. D. S.; Arawwawala, L. D. A. M. Comparative Phytochemical Analysis and Antioxidant Activities of Tamalakyadi Decoction with Its Modified Dosage Forms. *Evidence-Based Complementary and Alternative Medicine* **2019**, *2019*, 1−9.
(54) Ali, S.; Khan, M. R.; Irfanullah; Sajid, M.; Zahra, Z. Phytochemical Investigation and Antimicrobial Appraisal of Parrotiopsis Jacquemontiana (Decne) Rehder. *BMC Complement Altern. Med.* **2018**, *18* (1), 43.
(55) Godlewska, K.; Pacyga, P.; Najda, A.; Michalak, I. Investigation of Chemical Constituents and Antioxidant Activity of Biologically Active Plant-Derived Natural Products. *Molecules* **2023**, *28* (14), 5572.
(56) Le Thi, V.-A.; Nguyen, N.-L.; Nguyen, Q.-H.; Van Dong, Q.; Do, T.-Y.; Nguyen T, K.-O. Phytochemical Screening and Potential Antibacterial Activity of Defatted and Nondefatted Methanolic Extracts of Xao Tam Phan (Paramignya Trimera (Oliv.) Guillaum) Peels against Multidrug-Resistant Bacteria. *Scientifica* **2021**, *2021*, 4233615.
(57) Das, B. K.; Al-Amin, M. M.; Russel, S. M.; Kabir, S.; Bhattacherjee, R.; Hannan, J. M. Phytochemical Screening and

Evaluation of Analgesic Activity of Oroxylum indicum. *Indian J. Pharm. Sci.* **2014**, *76*, 571−575.
(58) Alhadhrami, A.; Mohamed, G. G.; Sadek, A. H.; Ismail, S. H.; Ebnalwaled, A. A.; Almalki, A. S. A. Behavior of Silica Nanoparticles Synthesized from Rice Husk Ash by the Sol−Gel Method as a Photocatalytic and Antibacterial Agent. *Materials* **2022**, *15* (22), 8211.
(59) Shrestha, D.; Nayaju, T.; Kandel, M. R.; Pradhananga, R. R.; Park, C. H.; Kim, C. S. Rice Husk-Derived Mesoporous Biogenic Silica Nanoparticles for Gravity Chromatography. *Heliyon* **2023**, *9* (4), No. e15142.
(60) Hoerudin; Setyawan, N.; Suismono; Purwaningsih, H.; Apriliani, N. Morphology, Extraction Yield, and Properties of Biogenic Silica Nanoparticles from Indonesian Rice Husk as Influenced by Solvent Type and Aging Time. *IOP Conf. Ser.: Earth Environ. Sci.* **2022**, *1024* (1), No. 012076.
(61) Kumar, A.; Verma, L. M.; Sharma, S.; Singh, N. Zinc Oxide Nanoparticles (ZnO NPs) Stabilized by Phytocellulose Derived Biopolymer and Their Bipartite Interaction Studies with Agriculturally Important Microbes/Raphanus Sativus (L.) Seeds. *Ceram. Int.* **2023**, *49* (24), 39771−39787.
(62) Rodríguez-Martínez, J.; Sánchez-Martín, M.-J.; Valiente, M. Efficient Controlled Release of Cannabinoids Loaded in γ-CD-MOFs and DPPC Liposomes as Novel Delivery Systems in Oral Health. *Microchim. Acta* **2023**, *190* (4), 125.
(63) Biradar, A. I.; Sarvalkar, P. D.; Teli, S. B.; Pawar, C. A.; Patil, P. S.; Prasad, N. R. Photocatalytic Degradation of Dyes Using One-Step Synthesized Silica Nanoparticles. *Materials Today: Proceedings* **2021**, *43*, 2832−2838.
(64) Sharma, S. K.; Sharma, A. R.; Pamidimarri, S. D. V. N.; Gaur, J.; Singh, B. P.; Sekar, S.; Kim, D. Y.; Lee, S. S. Bacterial Compatibility/Toxicity of Biogenic Silica (b-SiO2) Nanoparticles Synthesized from Biomass Rice Husk Ash. *Nanomaterials* **2019**, *9* (10), 1440.
(65) Nandanwar, R.; Singh, P.; Haque, F. Synthesis and Characterization of SiO2 Nanoparticles by Sol-Gel Process and Its Degradation of Methylene Blue. *ACSJ.* **2015**, *5* (1), 1−10.
(66) Verma, L. M.; Kumar, A.; Kumar, A.; Singh, G.; Singh, U.; Chaudhary, S.; Kumar, S.; Sanwaria, A. R.; Ingole, P. P.; Sharma, S. Green Chemistry Routed Sugar Press Mud for (2D) ZnO Nanostructure Fabrication, Mineral Fortification, and Climate-Resilient Wheat Crop Productivity. *Sci. Rep* **2024**, *14* (1), 4074.
(67) Singh, G.; Arora, H.; Hariprasad, P.; Sharma, S. Development of Clove Oil Based Nanoencapsulated Biopesticide Employing Mesoporous Nanosilica Synthesized from Paddy Straw via Bioinspired Sol-Gel Route. *Environ. Res.* **2023**, *220*, No. 115208.
(68) Ihssen, J.; Jovanovic, N.; Sirec, T.; Spitz, U. Real-Time Monitoring of Extracellular ATP in Bacterial Cultures Using Thermostable Luciferase. *PLoS One* **2021**, *16* (1), No. e0244200.
(69) Ilesanmi, O. I.; Adekunle, A. E.; Omolaiye, J. A.; Olorode, E. M.; Ogunkanmi, A. L. Isolation, optimization and molecular characterization of lipase producing bacteria from contaminated soil. *Scientific African* **2020**, *8*, No. e00279.
(70) Xu, X.; Cheng, W.; Liu, X.; You, H.; Wu, G.; Ding, K.; Tu, X.; Yang, L.; Wang, Y.; Li, Y.; Gu, H.; Wang, X. Selenate Reduction and Selenium Enrichment of Tea by the Endophytic Herbaspirillum Sp. Strain WT00C. *Curr. Microbiol.* **2020**, *77* (4), 588−601.
(71) Nasuha Nadhirah, N.; Anuar Kamaruddin, M.; Nazmi Ismail, M. Removal of Organic Constituents and Bacteria Count Disinfection from Fish Processing Wastewater by Using Ionic Cupric Copper. *IOP Conf. Ser.: Mater. Sci. Eng.* **2020**, *864* (1), No. 012023.
(72) Bankier, C.; Cheong, Y.; Mahalingam, S.; Edirisinghe, M.; Ren, G.; Cloutman-Green, E.; Ciric, L. A Comparison of Methods to Assess the Antimicrobial Activity of Nanoparticle Combinations on Bacterial Cells. *PLoS One* **2018**, *13* (2), No. e0192093.
(73) Rajeshkumar, S.; Menon, S.; Venkat Kumar, S.; Tambuwala, M. M.; Bakshi, H. A.; Mehta, M.; Satija, S.; Gupta, G.; Chellappan, D. K.; Thangavelu, L.; Dua, K. Antibacterial and Antioxidant Potential of Biosynthesized Copper Nanoparticles Mediated through Cissus Arnotiana Plant Extract. *Journal of Photochemistry and Photobiology B: Biology* **2019**, *197*, No. 111531.
(74) Arafa, M. G.; El-Kased, R. F.; Elmazar, M. M. Thermoresponsive Gels Containing Gold Nanoparticles as Smart Antibacterial and Wound Healing Agents. *Sci. Rep.* **2018**, *8* (1), No. 13674.
(75) Wu, H.; Ong, Z. Y.; Liu, S.; Li, Y.; Wiradharma, N.; Yang, Y. Y.; Ying, J. Y. Synthetic *β*-Sheet Forming Peptide Amphiphiles for Treatment of Fungal Keratitis. *Biomaterials* **2015**, *43*, 44−49.
(76) Pal, S.; Tak, Y. K.; Song, J. M. Does the Antibacterial Activity of Silver Nanoparticles Depend on the Shape of the Nanoparticle? A Study of the Gram-Negative Bacterium *Escherichia Coli*. *Appl. Environ. Microbiol.* **2007**, *73* (6), 1712−1720.
(77) Bellani, L.; Giorgetti, L.; Riela, S.; Lazzara, G.; Scialabba, A.; Massaro, M. Ecotoxicity of Halloysite Nanotube−Supported Palladium Nanoparticles in *Raphanus Sativus* L. *Environ. Toxicol. Chem.* **2016**, *35* (10), 2503−2510.
(78) Acharya, P.; Jayaprakasha, G. K.; Crosby, K. M.; Jifon, J. L.; Patil, B. S. Nanoparticle-Mediated Seed Priming Improves Germination, Growth, Yield, and Quality of Watermelons (*Citrullus lanatus*) at Multi-Locations in Texas. *Sci. Rep* **2020**, *10* (1), 5037.
(79) Khan, M. A. H.; Baset Mia, Md. A.; Quddus, Md. A.; Sarker, K. K.; Rahman, M.; Skalicky, M.; Brestic, M.; Gaber, A.; Alsuhaibani, A. M.; Hossain, A. Salinity-Induced Physiological Changes in Pea (*Pisum Sativum* L.): Germination Rate, Biomass Accumulation, Relative Water Content, Seedling Vigor and Salt Tolerance Index. *Plants* **2022**, *11* (24), 3493.
(80) Devi, D.; Gupta, S. B.; Mishra, B. K. Effect of Plant Growth Promoting Rhizobacteria on Seed Germination Behavior and Seedling Vigour of Cumin. *J. Pharmacogn. Phytochem.* **2020**, *9*, 2284−2288.
(81) Kandasamy, S.; Weerasuriya, N.; Gritsiouk, D.; Patterson, G.; Saldias, S.; Ali, S.; Lazarovits, G. Size Variability in Seed Lot Impact Seed Nutritional Balance, Seedling Vigor, Microbial Composition and Plant Performance of Common Corn Hybrids. *Agronomy* **2020**, *10* (2), 157.
(82) Abdul-Baki, A. A.; Anderson, J. D. Vigor Determination in Soybean Seed by Multiple Criteria [1]. *Crop Science* **1973**, *13* (6), 630−633.
(83) Nazeer, H.; Rauf, M.; Gul, H.; Yaseen, T.; Shah, A. A.; Rehman, K. U. Salt stress affects germination and seedling establishment in different wheat (Triticum aestivum L.) varieties. *J. Pure Appl. Agric.* **2020**, *5*, 42−51.
(84) Pour-Aboughadareh, A.; Ahmadi, J.; Mehrabi, A. A.; Etminan, A.; Moghaddam, M.; Siddique, K. H. M. Physiological Responses to Drought Stress in Wild Relatives of Wheat: Implications for Wheat Improvement. *Acta Physiol Plant* **2017**, *39* (4), 106.
(85) Bewick, V.; Cheek, L.; Ball, J. [No Title Found]. *Crit Care* **2003**, *7* (6), 451.
(86) Khatiwora, E.; Adsul, V. B.; Torane, R. C.; Gaikwad, S.; Deshpande, N. R.; Kashalkar, R. V. Spectroscopic determination of total phenol and flavonoid contents of *Citrus limon* peel from north eastern region of India. *J. Drug Delivery Ther.* **2017**, *7* (1), 21−24.
(87) Baba, S. A.; Malik, S. A. Determination of Total Phenolic and Flavonoid Content, Antimicrobial and Antioxidant Activity of a Root Extract of *Arisaema Jacquemontii* Blume. *Journal of Taibah University for Science* **2015**, *9* (4), 449−454.
(88) Yahyaoui, A.; Djebar, M. R.; Khene, L.; Bouarroudj, T.; Khali, H.; Bourayou, C. Assessment of exposure wheat Triticum aestivum L. to zinc oxide nanoparticles (ZnO): evaluation of oxidative damage. *Stud. Univ. "Vasile Goldis", Ser. Stiint. Vietii* **2017**, *27*, 271−280.
(89) Iftikhar, N.; Perveen, S. Riboflavin (Vitamin B2) Priming Modulates Growth, Physiological and Biochemical Traits of Maize (Zea Mays L.) under Salt Stress. *Pak. J. Bot.* **2024**, *56* (4). DOI: 10.30848/PJB2024-4(22)
(90) Eman Gökseven, Ş.B.; Kıran, S.; Ellialtıoğlu, Ş.Ş. Acid and Chelate Applications on Some Morphophysiological Properties and Antioxidant Enzyme Activities of Ornamental Cabbage (Brassica Oleracea Var. Acephala) under Boron Stress. *Soil Studies* **2022**, *11* (2), 85−95.

https://doi.org/10.1021/acsomega.4c08152
ACS Omega 2025, 10, 5537−5553

(91) Viena, V.; Elvitriana; Wardani, S. Application of Banana Peels Waste as Adsorbents for the Removal of CO_2, NO, NO_x, and SO_2 Gases from Motorcycle Emissions. *IOP Conf. Ser.: Mater. Sci. Eng.* **2018**, *334*, No. 012037.
(92) Cruz Shannen Lyka, S.; Pamintuan Francheska Edelle Lein, G.; Villanueva Ronan, B.; Munoz Jonathan, C.; Cruz Gil, G. Banana and Orange Peel Powder as Partial Cement Replacement Materials. A Comparative Analysis on Its Individual Influence on the Physico-mechanical Properties of Cement. *Chem. Eng. Trans.* **2023**, *106*, 433−438.
(93) Memon, J. R.; Memon, S. Q.; Bhanger, M. I.; El-Turki, A.; Hallam, K. R.; Allen, G. C. Banana Peel: A Green and Economical Sorbent for the Selective Removal of Cr(VI) from Industrial Wastewater. *Colloids Surf., B* **2009**, *70* (2), 232−237.
(94) Sapawe, N.; Surayah Osman, N.; Zulkhairi Zakaria, M.; Amirul Shahab Syed Mohamad Fikry, S.; Amir Mat Aris, M. Synthesis of Green Silica from Agricultural Waste by Sol-Gel Method. *Materials Today: Proceedings* **2018**, *5* (10), 21861−21866.
(95) Anhwange, B. A.; Ugye, T. J.; Nyiaatagher, T. D. Chemical composition of Musa sapientum (banana) peels. *EJEAFChe, Electronic J. Environ., Agric. Food Chem.* **2009**, *8* (6), 437−442.
(96) Puraikalan, Y. Characterization of Proximate, Phytochemical and Antioxidant Analysis of Banana (Musa Sapientum) Peels/Skins and Objective Evaluation of Ready to Eat /Cook Product Made With Banana Peels. *Current Research in Nutrition and Food Science Journal* **2018**, *6* (2), 382−391.
(97) Olakunle, O.; Deborah, J.; Irene, O. Antifungal Activity and Phytochemical Analysis of Selected Fruit Peels. *J. Biol. Med.* **2019**, *3* (1), 040−043.
(98) Kibria, A. A.; Kamrunnessa; Rahman, Md. M.; Kar, A. Extraction and Evaluation of Phytochemicals from Banana Peels (*Musa Sapientum*) and Banana Plants (*Musa Paradisiaca*). *Malaysian Journal of Halal Research* **2019**, *2* (1), 22−26.
(99) Bashir, F.; Hassan, A.; Mushtaq, A.; Rizwan, S.; Jabeen, U.; Raza, A.; Anjum, S.; Masood, A. Phytochemistry and Antimicrobial Activities of Different Varieties of Banana (*Musa Acuminate*) Peels Available in Quetta City. *Polym. J. Environ. Stud.* **2021**, *30* (2), 1531−1538.
(100) Memon, J. R.; Memon, S. Q.; Bhanger, M. I.; Memon, G. Z.; El-Turki, A.; Allen, G. C. Characterization of Banana Peel by Scanning Electron Microscopy and FT-IR Spectroscopy and Its Use for Cadmium Removal. *Colloids Surf., B* **2008**, *66* (2), 260−265.
(101) Udochukwu, E. C.; Akpoviri, C. U. Morphological Characterization Of Banana Peel Powder As A Bio-Adsorbent For Waste Water Treatment. *Int. J. Eng.* **2022**, *1*, 1−6.
(102) Stanienda-Pilecki, K. J. The importance of Fourier-Transform Infrared Spectroscopy in the identification of carbonate phases differentiated in magnesium content. *Spectroscopy* **2019**, *34*, 32−42.
(103) Nasrazadani, S.; Eureste, E. *Application of FTIR for Quantitative Analysis of Lime*, Technical Report No. FHWA/tX-0815-9028-01-1; University of North Texas, 2008.
(104) LibreTexts, Chemistry. Infrared Spectroscopy Absorption Table. https://chem.libretexts.org/Ancillary_Materials/Reference/Reference_Tables/Spectroscopic_Reference_Tables/Infrared_Spectroscopy_Absorption_Table (accessed 2024-03-22).
(105) Nayak, P. P.; Datta, A. K. Synthesis of SiO2-Nanoparticles from Rice Husk Ash and Its Comparison with Commercial Amorphous Silica through Material Characterization. *Silicon* **2021**, *13* (4), 1209−1214.
(106) Adebisi, J. A.; Agunsoye, J. O.; Bello, S. A.; Haris, M.; Ramakokovhu, M. M.; Daramola, M. O.; Hassan, S. B. Green Production of Silica Nanoparticles from Maize Stalk. *Particulate Science and Technology* **2020**, *38* (6), 667−675.
(107) Barma, M. D.; Kannan, S. D.; Indiran, M. A.; Rajeshkumar, S.; Kumar, R. P. Antibacterial Activity of Mouthwash Incorporated with Silica Nanoparticles against S. Aureus, S. Mutans, E. Faecalis: An in-Vitro Study. *JPRI* **2020**, 25−33.
(108) Ali, A.; Saeed, S.; Hussain, R.; Afzal, G.; Siddique, A. B.; Parveen, G.; Hasan, M.; Caprioli, G. Synthesis and Characterization of Silica, Silver-Silica, and Zinc Oxide-Silica Nanoparticles for Evaluation of Blood Biochemistry, Oxidative Stress, and Hepatotoxicity in Albino Rats. *ACS Omega* **2023**, *8* (23), 20900−20911.
(109) Silmi, N. I.; Antasari, F. A.; et al. NPK Fertilizer With Slow Release Fly Ash. *J. Pure App Chem. Res.* **2018**, *7*, 1−11.
(110) Periakaruppan, R.; N, R. D.; Abed, S. A.; Vanathi, P.; Kumar, J. S. Production of Biogenic Silica Nanoparticles by Green Chemistry Approach and Assessment of their Physicochemical Properties and Effects on the Germination of Sorghum bicolor. *Silicon* **2023**, *15*, 4309−4316.
(111) Yadav, R. K.; Chauhan, P. Estimation of lattice strain in Mn-doped ZnO nanoparticles and its effect on structural and optical properties. *Indian J. Pure Appl. Phys.* **2020**, *57*, 881−890.
(112) Geetha, M. S.; Nagabhushana, H.; Shivananjaiah, H. N. Green Mediated Synthesis and Characterization of ZnO Nanoparticles Using Euphorbia Jatropa Latex as Reducing Agent. *Journal of Science: Advanced Materials and Devices* **2016**, *1* (3), 301−310.
(113) Tasleem, S.; Sabah, A.; Tahir, M.; Sabir, A.; Shabbir, A.; Nazir, M. Alkyl Silica Hybrid Nanowire Assembly in Improved Super-hydrophobic Membranes for RO Filtration. *ACS Omega* **2022**, *7* (5), 3940−3948.
(114) Verma, J. Analysis on Synthesis of Silica Nanoparticles and Its Effect on Growth of T. Harzianum & Rhizoctonia Species. *Biomed. J. Sci. Tech. Rep.* **2018**, *10* (4), 7890−7897.
(115) Maroušek, J.; Maroušková, A.; Periakaruppan, R.; Gokul, G. M.; Anbukumaran, A.; Bohatá, A.; Kříž, P.; Bárta, J.; Černý, P.; Olšan, P. Silica Nanoparticles from Coir Pith Synthesized by Acidic Sol-Gel Method Improve Germination Economics. *Polymers* **2022**, *14* (2), 266.
(116) Chandra, S.; Beaune, G.; Shirahata, N.; Winnik, F. M. A One-Pot Synthesis of Water Soluble Highly Fluorescent Silica Nanoparticles. *J. Mater. Chem. B* **2017**, *5* (7), 1363−1370.
(117) Darabi, H.; Adelifard, M.; Rajabi, Y. Characterization of Nonlinear Optical Refractive Index for Graphene Oxide−Silicon Oxide Nanohybrid Composite. *J. Nonlinear Optic. Phys. Mater.* **2019**, *28* (01), No. 1950005.
(118) Kaur, H.; Kaur, G. Spectroscopic and Quantum Chemical Computational Studies of Silica Nanocrystals Extracted from Rice Straw. *Silicon* **2022**, *14* (12), 6803−6816.
(119) Lee, J.-H.; El-Fiqi, A.; Jo, J.-K.; Kim, D.-A.; Kim, S.-C.; Jun, S.-K.; Kim, H.-W.; Lee, H.-H. Development of Long-Term Antimicrobial Poly(Methyl Methacrylate) by Incorporating Mesoporous Silica Nanocarriers. *Dental Materials* **2016**, *32* (12), 1564−1574.
(120) Balaure, P. C.; Boarca, B.; Popescu, R. C.; Savu, D.; Trusca, R.; Vasile, B. Ş.; Grumezescu, A. M.; Holban, A. M.; Bolocan, A.; Andronescu, E. Bioactive Mesoporous Silica Nanostructures with Anti-Microbial and Anti-Biofilm Properties. *Int. J. Pharm.* **2017**, *531* (1), 35−46.
(121) Joni, I. M.; Nulhakim, L.; Vanitha, M.; Panatarani, C. Characteristics of Crystalline Silica (SiO_2) Particles Prepared by Simple Solution Method Using Sodium Silicate (Na_2SiO_3) Precursor. *J. Phys.: Conf. Ser.* **2018**, *1080*, No. 012006.
(122) Stanley, R.; Nesaraj, A. S. Effect of surfactants on the wet chemical synthesis of silica nanoparticles. *Int. J. Appl. Sci. Eng.* **2014**, *12*, 9−21.
(123) Araichimani, P.; Prabu, K. M.; Kumar, G. S.; Karunakaran, G.; Surendhiran, S.; Shkir, M; AlFaify, S. Rice Husk-Derived Mesoporous Silica Nanostructure for Supercapacitors Application: A Possible Approach for Recycling Bio-Waste into a Value-Added Product. *Silicon* **2022**, *14* (15), 10129−10135.
(124) Idris, I.; Naddaf, M.; Harmalani, H.; Alshater, R.; Alsafadi, R. Efficacy of Olive Stones and Corncobs Crystalline Silica Nanoparticles (SiO2, NPs) Treatments on Potato Tuber Moths (Phthorimaea Operculella). *Silicon* **2023**, *15* (8), 3591−3598.
(125) Ramasamy, S. P.; Veeraswamy, D.; Ettiyagounder, P.; Arunachalam, L.; Devaraj, S. S.; Krishna, K.; Oumabady, S.; Sakrabani, R. New Insights Into Method Development and Characterization of Amorphous Silica From Wheat Straw. *Silicon* **2023**, *15* (12), 5049−5063.

(126) Hanna, S. B.; Mansour, T. S.; Ajiba, N. A. Processing and Characterization of Nano Silica and Iron Oxide Coated Silica Composites Extracted from Rice Hulls. *Silicon* **2023**, *15* (14), 6099−6111.

(127) Seroka, N. S.; Taziwa, R.; Khotseng, L. Green Synthesis of Crystalline Silica from Sugarcane Bagasse Ash: Physico-Chemical Properties. *Nanomaterials* **2022**, *12* (13), 2184.

(128) Hoffmann, F.; Cornelius, M.; Morell, J.; Fröba, M. Silica-Based Mesoporous Organic−Inorganic Hybrid Materials. *Angew. Chem. Int. Ed* **2006**, *45* (20), 3216−3251.

(129) Prabha, S.; Durgalakshmi, D.; Rajendran, S.; Lichtfouse, E. Plant-Derived Silica Nanoparticles and Composites for Biosensors, Bioimaging, Drug Delivery and Supercapacitors: A Review. *Environ. Chem. Lett.* **2021**, *19* (2), 1667−1691.

(130) Gordienko, A. S.; Kurdish, I. K. Surface Electrical Properties of Bacillus Subtilis Cells and the Effect of Interaction with Silicon Dioxide Particles. *Biophysics* **2007**, *52* (2), 217−219.

(131) Tian, B.; Liu, Y.; Chen, D. Adhesion Behavior of Silica Nanoparticles with Bacteria: Spectroscopy Measurements Based on Kinetics, and Molecular Docking. *J. Mol. Liq.* **2021**, *343*, No. 117651.

(132) Omardien, S.; Brul, S.; Zaat, S. A. J. Antimicrobial Activity of Cationic Antimicrobial Peptides against Gram-Positives: Current Progress Made in Understanding the Mode of Action and the Response of Bacteria. *Front. Cell Dev. Biol.* **2016**, *4*, 111.

(133) Sewell, E. W.; Brown, E. D. Taking Aim at Wall Teichoic Acid Synthesis: New Biology and New Leads for Antibiotics. *J. Antibiot.* **2014**, *67* (1), 43−51.

(134) Brown, S.; Santa Maria, J. P.; Walker, S. Wall Teichoic Acids of Gram-Positive Bacteria. *Annu. Rev. Microbiol.* **2013**, *67* (1), 313−336.

(135) Sharma, S. K.; Chiang, L. Y.; Hamblin, M. R. Photodynamic Therapy with Fullerenes *In Vivo* : Reality or a Dream? *Nanomedicine* **2011**, *6* (10), 1813−1825.

(136) Dorairaj, D.; Govender, N.; Zakaria, S.; Wickneswari, R. Green Synthesis and Characterization of UKMRC-8 Rice Husk-Derived Mesoporous Silica Nanoparticle for Agricultural Application. *Sci. Rep* **2022**, *12* (1), No. 20162.

(137) Taqdees, Z.; Khan, J.; Khan, W.-D.; Kausar, S.; Afzaal, M.; Akhtar, I. Silicon and Zinc Nanoparticles-Enriched Miscanthus Biochar Enhanced Seed Germination, Antioxidant Defense System, and Nutrient Status of Radish under NaCl Stress. *Crop & Pasture Science* **2022**, *73* (5), 556−572.

(138) Sun, D.; Hussain, H. I.; Yi, Z.; Rookes, J. E.; Kong, L.; Cahill, D. M. Mesoporous Silica Nanoparticles Enhance Seedling Growth and Photosynthesis in Wheat and Lupin. *Chemosphere* **2016**, *152*, 81−91.

(139) Zaheer, S.; Shehzad, J.; Chaudhari, S. K.; Hasan, M.; Mustafa, G. Morphological and Biochemical Responses of Vigna Radiata L. Seedlings Towards Green Synthesized SiO2 NPs. *Silicon* **2023**, *15* (14), 5925−5936.

(140) Mir, R. A.; Bhat, B. A.; Yousuf, H.; Islam, S. T.; Raza, A.; Rizvi, M. A.; Charagh, S.; Albaqami, M.; Sofi, P. A.; Zargar, S. M. Multidimensional Role of Silicon to Activate Resilient Plant Growth and to Mitigate Abiotic Stress. *Front. Plant Sci.* **2022**, *13*, No. 819658.

(141) Wang, L.; Ning, C.; Pan, T.; Cai, K. Role of Silica Nanoparticles in Abiotic and Biotic Stress Tolerance in Plants: A Review. *IJMS* **2022**, *23* (4), 1947.

(142) Sarkar, M. M.; Mathur, P.; Mitsui, T.; Roy, S. A Review on Functionalized Silica Nanoparticle Amendment on Plant Growth and Development under Stress. *Plant Growth Regul* **2022**, *98* (3), 421−437.

(143) Irfan, M.; Maqsood, M. A.; Rehman, H. U.; Mahboob, W.; Sarwar, N.; Hafeez, O. B. A.; Hussain, S.; Ercisli, S.; Akhtar, M.; Aziz, T. Silicon Nutrition in Plants under Water-Deficit Conditions: Overview and Prospects. *Water* **2023**, *15* (4), 739.

(144) Nano Silica Market Research Nano Silica Market Size, Share, Competitive Landscape and Trend Analysis Report by Product, by Application: Global Opportunity Analysis and Industry Forecast, 2022−2031. Report Code: A02110; Allied Market Research, 2022; pp 282. https://www.alliedmarketresearch.com/nano-silica-market (accessed 2024-04-22).

https://doi.org/10.1021/acsomega.4c08152
ACS Omega 2025, 10, 5537−5553